AD-A100 945 DAYTON UNIV OH RESEARCH INST F/G 21/8.2
NUMERICAL TECHNIQUES FOR SOLVING NONLINEAR INSTABILITY PROBLEMS--ETC(U)
APR 81 J D BAUM, J N LEVINE F04611-77-C-0042
UNCLASSIFIED UDR-TR-80-106 AFRPL-TR-80-78 NL

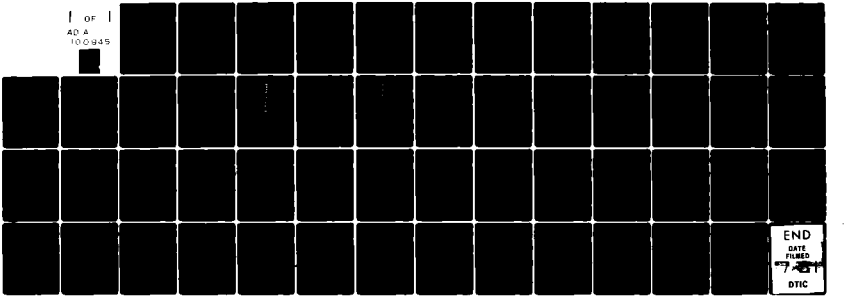

AFRPL-TR-80-78

UDR-TR-80-106

LEVEL II 3

NUMERICAL TECHNIQUES FOR SOLVING NONLINEAR INSTABILITY PROBLEMS IN SMOKELESS TACTICAL SOLID ROCKET MOTORS

J. D. BAUM
University of Dayton
Research Institute
Dayton, Ohio 45469

J. N. LEVINE
Air Force Rocket Propulsion Laboratory
Edwards Air Force Base, California 93534

April 1981

Final Report

Prepared for:

Air Force Rocket Propulsion Laboratory
Director of Science and Technology
Air Force Systems Command
Edwards Air Force Base, California 93523

NOTICE

"When U.S. Government drawings specifications, or other data are used for any purpose other than a definitely related government procurement operation, the Government thereby incurs no responsibility nor any obligation whatsoever, and the fact that the Government may have formulated, furnished, or in any other way supplied the said drawings, specifications or other data, is not to be regarded by implication or otherwise, or in any manner as licensing the holder or any other person or corporation, or conveying any rights or permission to manufacture, use, or sell any patented invention that may in any way be related thereto."

This report was submitted by the University of Dayton Research Institute, Dayton, OH 45469 under Contract Number F04611-77-C-0042, Job Order Number 99930ZC with the Air Force Rocket Propulsion Laboratory, Edwards Air Force Base, CA 93523. This report includes work done from 15 February, 1980 to 30 September, 1980. The research was performed at the Air Force Propulsion Laboratory, Edwards Air Force Base, California. The principal investigator was Dr. Joseph D. Baum. Project Manager was Dr. Lawrence P. Quinn and the Task Manager was J. N. Levine.

This technical report is approved for release and distribution in accordance with the distribution statement on the cover and on the DD Form 1473.

LAWRENCE P. QUINN

FOR THE COMMANDER

JAMES T. EDWARDS

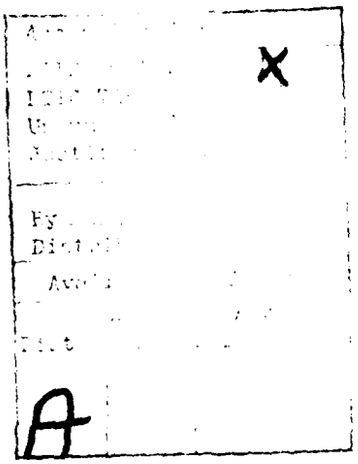

UNCLASSIFIED

SECURITY CLASSIFICATION OF THIS PAGE (When Data Entered)

REPORT DOCUMENTATION PAGE

READ INSTRUCTIONS BEFORE COMPLETING FORM

1. REPORT NUMBER: AFRPL-TR-80-78	2. GOVT ACCESSION NO.: AD-A100 945
3. RECIPIENT'S CATALOG NUMBER:	
4. TITLE (and Subtitle): Numerical Techniques for Solving Nonlinear Instability Problems in Smokeless Tactical Solid Rocket Motors	5. TYPE OF REPORT & PERIOD COVERED: Final Report, 15 February 1980 - 30 September 1980
	6. PERFORMING ORG. REPORT NUMBER: UDR-TR-80-106
7. AUTHOR(S): Dr. Joseph D. Baum *Mr. J. N. Levine	8. CONTRACT OR GRANT NUMBER(S): F04611-77-C-0042
9. PERFORMING ORGANIZATION NAME AND ADDRESS: University of Dayton Research Institute Dayton, OH 45469	10. PROGRAM ELEMENT, PROJECT, TASK AREA & WORK UNIT NUMBERS: 2308M1UJ
11. CONTROLLING OFFICE NAME AND ADDRESS: Air Force Rocket Propulsion Laboratory/XRX Edwards Air Force Base, California 93523	12. REPORT DATE: October 1980 13. NUMBER OF PAGES: 47
14. MONITORING AGENCY NAME & ADDRESS (if different from Controlling Office): —	15. SECURITY CLASS (of this report): Unclassified 15a. DECLASSIFICATION/DOWNGRADING SCHEDULE

16. DISTRIBUTION STATEMENT (of this Report)

Approved for public release; Distribution unlimited.

17. DISTRIBUTION STATEMENT (of the abstract entered in Block 20, if different from Report)

Approved for public release; Distribution unlimited.

18. SUPPLEMENTARY NOTES

*Air Force Rocket Propulsion Laboratory
Edwards Air Force Base, CA 93534

19. KEY WORDS (Continue on reverse side if necessary and identify by block number)

Solid Rocket Motors
Combustion Instability
Nonlinear Instability
Numerical Analysis
Finite Difference Skin
Hyperbolic Equation
Two-phase Flow

20. ABSTRACT (Continue on reverse side if necessary and identify by block number)

The results of an investigation to select a satisfactory numerical method for calculating the propagation of steep fronted shock like waveforms in a solid rocket motor combustion chamber are presented. A number of different numerical schemes were evaluated by comparing the results obtained for three problems: the shock tube problem, the linear wave equation, and nonlinear wave propagation in a closed tube. The most promising method--a combination of the Lax-Wendroff, Hybrid and Artificial Compression techniques was incorporated into an existing non-linear instability program. The capability of the

DD FORM 1 JAN 73 1473 EDITION OF 1 NOV 65 IS OBSOLETE

UNCLASSIFIED

SECURITY CLASSIFICATION OF THIS PAGE (When Data Entered)

20. ABSTRACT (Continued)

modified program to treat steep fronted wave instabilities in low smoke tactical motors was verified by solving a number of motor test cases with disturbance amplitudes as high as 80% of the mean pressure.

SUMMARY

The objective of the research work presented in this report was to evaluate existing finite difference methods and select and apply the one most appropriate for computing the propagation of multiple shock waves in a two-phase rocket combustion chamber.

In order to be acceptable for the intended application, a finite difference integration scheme must: preserve the high frequency content of the waveforms; be relatively nondissipative and nondispersive after many wave cycles; be capable of describing a shock wave as a sharp discontinuity; and be capable of properly treating the reflection of shock waves from boundaries and the partial reflection and transmission of discontinuities.

The finite difference schemes of the Split Coefficient method, the λ-scheme, Rubin and Burstein, MacCormack, Lax-Wendroff, Godunov, Rusanov, the Flux-Corrected-Transport scheme of Boris and Book, Chorin's implementation of Glimm's Method, the Hybrid scheme of Harten and Zwas and the Artificial-Compression method of Harten were evaluated. All of these schemes are finite difference approximations to the derivatives arising in the conservation laws and can treat an arbitrary system of conservation laws.

As a first step in evaluating the potential of these schemes, they were utilized in the solution of the shock tube problem for the one-dimensional Eulerian form of the gas dynamic conservation equations for an inviscid, non heat-conducting fluid and for the solution of the linear wave equation problem. The final test problem was the solution of the one-dimensional nonlinear hyperbolic equations describing finite amplitude wave and shock propagation in a closed end tube. In addition, the ability to spectrally analyze the computed results was developed. This capability simplifies the interpretation of the complex waveforms and facilitates comparisons among the various finite difference integration schemes.

The results of applying several of the above mentioned schemes to the last test case are presented and discussed in this report. It had been concluded that for the present problem, a method based upon the combination of the Lax-Wendroff, Hybrid and Artificial Compression scheme was found to be superior to the other schemes tested. This scheme was incorporated into the nonlinear instability program developed by Levine and Culick that described the combustion and flow inside a solid rocket motor. Finally, the ability of this scheme to treat various initial disturbances in a solid rocket motor such as a first mode disturbance and standing or traveling pulses, is demonstrated.

TABLE OF CONTENTS

LIST OF ILLUSTRATIONS

SECTION 1
INTRODUCTION

This report presents the results of an investigation designed to select a satisfactory method for computing the propagation of steep-fronted shocklike waveforms in a two-phase rocket combustion chamber.

Tactical solid rocket motors are frequently subject to a combustion instability problem at some point in the design cycle. When instability is encountered, it can take one of several forms, e.g., linear or nonlinear, longitudinal or tangential. Over the last twenty years, considerable resources have been expended to understand, predict, control, and eliminate combustion instability in solid rocket motors. Most of this effort has been devoted to linear instability problems, and as a result, such problems can now be treated in a rational, cost effective manner. In comparison, little work has been accomplished towards the understanding and resolution of nonlinear combustion instability problems. Thus, when nonlinear instabilities are encountered, the solution is too often an expensive cut-and-try process.

Linear instability is characterized by small amplitude, sinusoidal oscillations that originate from the amplification of infinitesimal random disturbances in the motor chamber. Nonlinear instability is usually characterized by large amplitude oscillations having steep-fronted, shocklike waveforms, and is initiated by random finite amplitude events such as the expulsion of an igniter or insulation fragment through the nozzle. Nonlinear instabilities are modeled using both "exact" and "approximate" mathematical techniques. The "exact" methods of Levine and Culick,[1] and those of Kooker and Zinn,[2] seek to solve numerically the nonlinear partial differential equations governing both the mean and time dependent flow in the combustion chamber, as well as the combustion response of the solid propellant. The "approximate" methods of Culick,[3] and of Powell, et.al.,[4] utilize

---

1. Levine, J. N. and Culick, F. E. C., "Nonlinear Analysis of Solid Rocket Combustion Instability," AFRPL Technical Report TR-74-45, October 1974.

2. Kooker, D. E. and Zinn, B. T., "Numerical Solution of Axial Instabilities in Solid Propellant Rocket Motors," 10th JANNAF Combustion Meeting, Vol. I, Naval War College, Newport, R.I., August 1973, CPIA Pub. 243.

3. Culick, F. E. C., "Nonlinear Behavior of Acoustic Waves in Combustion Chambers," 10th JANNAF Combustion Meeting, Vol. I, Naval War College, Newport, R.I., August 1973.

4. Powell, E. A., Padmanaboan, M. S., and Zinn, B. T., "Approximate Nonlinear Analysis of Solid Rocket Motors and T-Burners," AFRPL-TR-77-46, July 1977.

perturbation techniques and harmonic analysis to reduce the governing differential equations. Each of these methods has certain advantages, disadvantages, and limitations. The two classes of approaches complement each other, and efforts to develop both further are warranted.

The existing "exact" nonlinear instability programs were developed about seven years ago and are not capable of treating the multiple shock steep-fronted type of instabilities that occur in reduced and minimum smoke tactical motors developed since then. The objective of the present research is to extend and improve the "exact" model developed by Levine, et. al.,[5] in reference 1 to the point where it can be used by motor designers as a tool to aid in the efficient resolution of such nonlinear longitudinal instability problems. The first phase of this research, the results of which are reported herein, was devoted to improving the finite difference numerical technique used to solve the equations governing wave propagation in the combustion chamber.

In order to be acceptable for the intended application, a finite difference technique must (a) preserve the high-frequency content of the waveforms; (b) be relatively nondissipative and non-dispersive after many wave cycles, (c) be capable of describing a shock wave as a sharp discontinuity without generating overshoots or undershoots upon crossing the discontinuity; and (d) be capable of partial reflection and transmission at area discontinuities. It should be pointed out that in solving a combustion instability problem, numerically induced pre- and post-shock "wiggles" do not just impair the accuracy of the solution but could also falsely "trigger" nonlinear instabilities and force the scheme to pick a nonphysical solution.

It is very difficult for any single finite difference scheme to satisfy all of the aforementioned requirements simultaneously. For example, several artificial viscosity schemes[6] have been developed to damp pre- and post-shock oscillations. However, such artificially introduced diffusion also smears out the discontinuity and eventually damps the high-frequency modes that are part of the physical flow field inside the motor. Moreover, such artificial damping can be comparable in magnitude to the usual net gains or losses of acoustic energy in rocket motors; hence, its presence would seriously limit the validity of the results. In addition, use of an artificial viscosity would hamper efforts to determine

---

5. Levine and Culick, Op. Cit.

6. Lapidus, A., "A Detached Shock Calculation by Second Order Finite Differences," J. of Comp. Phys., Vol. 2, pp. 154-177, 1967.

the actual damping of gas phase oscillations in metallized solid propellant rocket motors. In this connection, it should be pointed out that shock-fitting schemes[7] that treat the shock as an internal boundary are impractical for this application, due to the large number of shocks traveling, interacting, and reflecting inside variable cross-sectional area motors. Similarly, finite difference schemes (such as the λ-scheme[8] or the split-coefficient method[9]) that are modeled after and exploit the mathematical theory of the method of characteristics are impractical for our specific problem. Shock-capturing implicit difference schemes offer no particular advantage for the present problem, since the physical problem of interest requires time resolution consistent with the stability restrictions of explicit methods.

Six or seven years ago, the task of finding a suitable finite difference scheme would have been virtually impossible, as then existing methods such as MacCormack,[10] Lax-Wendroff,[11] Godunov,[12] etc., lacked the required qualities. Since then, however, several special schemes designed to achieve shock resolution without "wiggles" were developed. Among them are the Flux-Corrected-Transport scheme of Boris and Book,[13] Chorin's[14] implementation of Glimm's method, the Upstream Centered scheme

---

7. Moretti, G., "The Choice of a Time Dependent Technique in Gas Dynamics," PIBAL Report 69-26, Polytechnical Institute of Brooklyn, July 1969.

8. Moretti, G., "The g-Scheme," Computer and Fluids, Vol. 17, 1979, pp. 191-205.

9. Chakravarthy, S. R., Anderson, D. A., and Salas, M. D., "The Split-Coefficient Matrix Method for Hyperbolic Systems of Gas Dynamic Equations," AIAA paper 80-0268, presented at the 18th Aerospace Sciences Meeting, Pasadena, California, January 14-16, 1980.

10. MacCormack, R. W., "Proceedings of the Second International Conference on Numerical Methods in Fluid Dynamics," lecture notes in Physics, (M. Holt, Ed., Vol. 8, Springer-Verlag, New York, 1971.

11. Lax, P. D. and Wendroff, B., "System of Conservation Laws," Comm. Pure Appl. Math., Vol. 13, 1960, pp. 217-237.

12. Godunov, S. K., "Finite Difference Methods for Numerical Computations of Discontinuous Solutions of Equations of Fluid Dynamics," Math. Sys. Vol. 47, 1959, pp. 271-295.

13. Boris, J. P. and Book, D. L., "Flux Corrected Transport III, Minimum Error F. C. T. Algorithms," J. of Comp. Physics, Vol. 20, 1976, pp. 397-431.

14. Chorin, A. J., "Random Choice Solution of Hyperbolic System," J. of Comp. Physics, Vol. 22, 1976, pp. 517-533.

of Van-Leer,[15] the Hybrid Scheme of Harten and Zwas,[16] and the Artificial Compression Scheme of Harten.[17] All of these schemes are finite difference approximations to the derivatives arising in the conservation laws and can treat an arbitrary system of conservation laws. In addition, they are *all fixed grid methods and can automatically* handle interactions between waves of different families. In order to evaluate the suitability of the aforementioned techniques for the present purpose, their ability to treat a number of simpler, but related, problems was examined. The results of this investigation are summarized in Section 3. The finite difference scheme judged most promising was then incorporated into the nonlinear instability program described by Levine and Culick[18]. The results of a number of nonlinear instability solutions are presented to demonstrate the effectiveness of the new technique.

---

15. Van Leer, B., "Towards the Ultimate Conservative Difference Scheme III, Upstream-Centered Finite-Difference Scheme for Ideal Compressible Flows," J. of Comp. Physics, Vol. 3, 1977, pp. 263-275.

16. Harten, A. and Zwas, G., "Self Adjusting Hybrid Schemes for Shock Computations," J. of Comp. Physics, Vol. 9, 1972, pp. 568-583.

17. Harten, A., "The Artificial Compression Method for Computation of Shocks and Contact Discontinuities: III, Self Adjusting Hybrid Schemes," AFOSR Technical Report TR-77-0659, March 1977.

18. Levine and Culick, Op. Cit.

SECTION 2
TEST PROBLEM RESULTS

2.1 SHOCK TUBE PROBLEM

As a first step in evaluating the various finite difference schemes, they were used to solve the shock tube problem for the one-dimensional Eulerian form of the gas dynamic conservation equations for an inviscid, non-heat-conducting fluid. These solutions were used to rate the difference schemes based upon such criteria as resolution of the shock (i.e., number of mesh points needed to describe the shock discontinuity), diffusion and smearing of the shock and the contact discontinuities with time, stability, effect of Courant number, and computation time.

The results of the shock tube test case demonstrated the superiority of the recently developed techniques[19-23] over earlier methods.[24,25] Based on the previously mentioned criteria, the best method was a combination of three techniques. The basic scheme of Lax-Wendroff[26] was combined with a Hydrid scheme[27] and the Artificial Compression Method.[28] This method (LW+H+ACM) was capable of producing very sharp shock waves, without pre- or post-shock wiggles.

2.2 LINEAR WAVE EQUATION

The various finite difference methods were also employed to solve a second problem, i.e., the linear wave equation. The results were used to evaluate the relative diffusive and dispersive errors of the schemes for harmonic standing wave propagation after many wave

---

19. Boris, Op. Cit.
20. Chorin, Op. Cit.
21. Van Leer, Op. Cit.
22. Harten and Zwas, Op. Cit.
23. Harten, Op. Cit.
24. MacCormack, Op. Cit.
25. Godunov, Op. Cit.
26. Lax and Wendroff, Op. Cit.
27. Harten and Zwas, Op. Cit.
28. Harten, Op. Cit.

cycles. This problem was also used to assess the ease of implementation of boundary conditions for the techniques considered.

The linear wave equation solutions demonstrated that the magnitude of the diffusive and dispersive errors varied significantly from one method to another. The LW+II+AVM combination method produced excellent solutions to this problem, with little error evident after many wave cycles.

2.3. WAVE PROPAGATION IN A CLOSED TUBE

The final test leading to the selection of a method to be utilized in the nonlinear instability program was the solution of the one-dimensional, nonlinear hyperbolic equations describing finite amplitude wave and shock propagation in a closed end tube. By establishing different initial conditions, it was possible to compare results obtained with the various techniques for problems ranging from almost linear (small initial disturbances) to highly nonlinear (large disturbances) conditions, over a large number of wave cycles. In addition, results obtained with these techniques were compared for problems such as interactions of different wave families and the effect of change in grid size and Courant number upon the frequency content of the scheme.

Some of the results of the last test problem--finite amplitude wave in a closed tube--will be presented to illustrate some of the differences between the techniques. As a result of the numerical error associated with finite difference methods, each technique acts as a numerical filter. The "filtering" effect of each of the techniques is a different function of frequency, mesh size, etc. To enhance the ability to discern these differences, the results of the test problems were spectrally analyzed.

Figures 1, 2, and 3 demonstrate the effect of numerical technique on the time evolution of acoustic pressure amplitude at an end of a closed tube. The solutions were initiated with a first harmonic standing wave perturbation having an amplitude of 20% of the mean pressure. The numerical schemes used in the figures were the LW+II+AVM method (Fig. 1), the MacCormack scheme (Fig. 2) and the Rubin and Burstein scheme[29] (Fig. 3). The evolution of post-shock wiggles into erroneous higher harmonics is evident in the latter two cases. Spectral analyses of the results shown in Figures 1, 2, and 3 are presented in Figures 4, 5, and 6 respectively.

---

29. Rubin, E. L. and Burstein, S. Z., "Difference Methods for the Inviscid and Viscous Equations of a Compressible Gas," Journal of Computational Physics, Vol. 2, 1967, pp. 178-96.

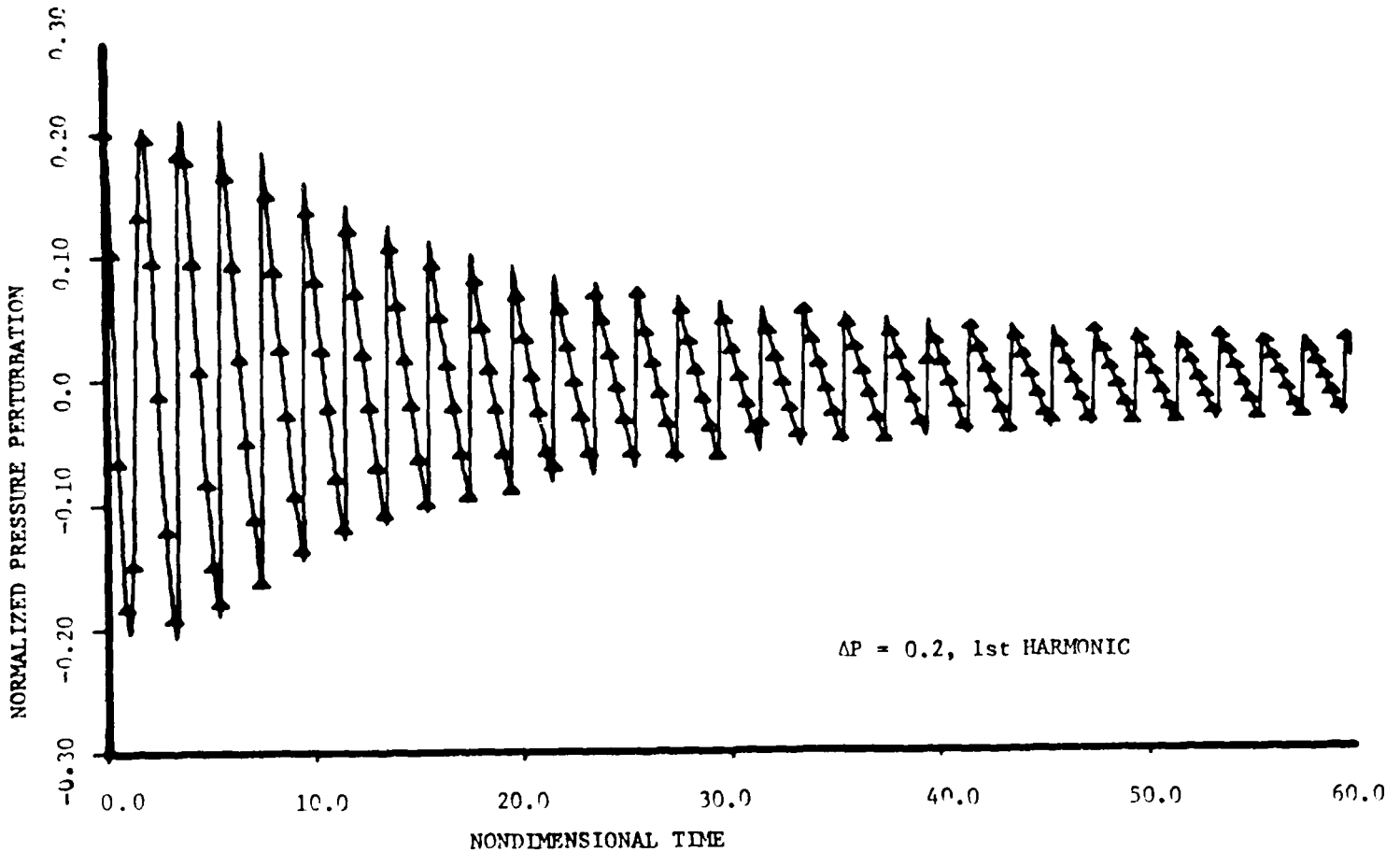

Figure 1. Time Evolution of Pressure Oscillations at an end of a Tube (Lax-Wendroff+Hybrid+ACM Scheme).

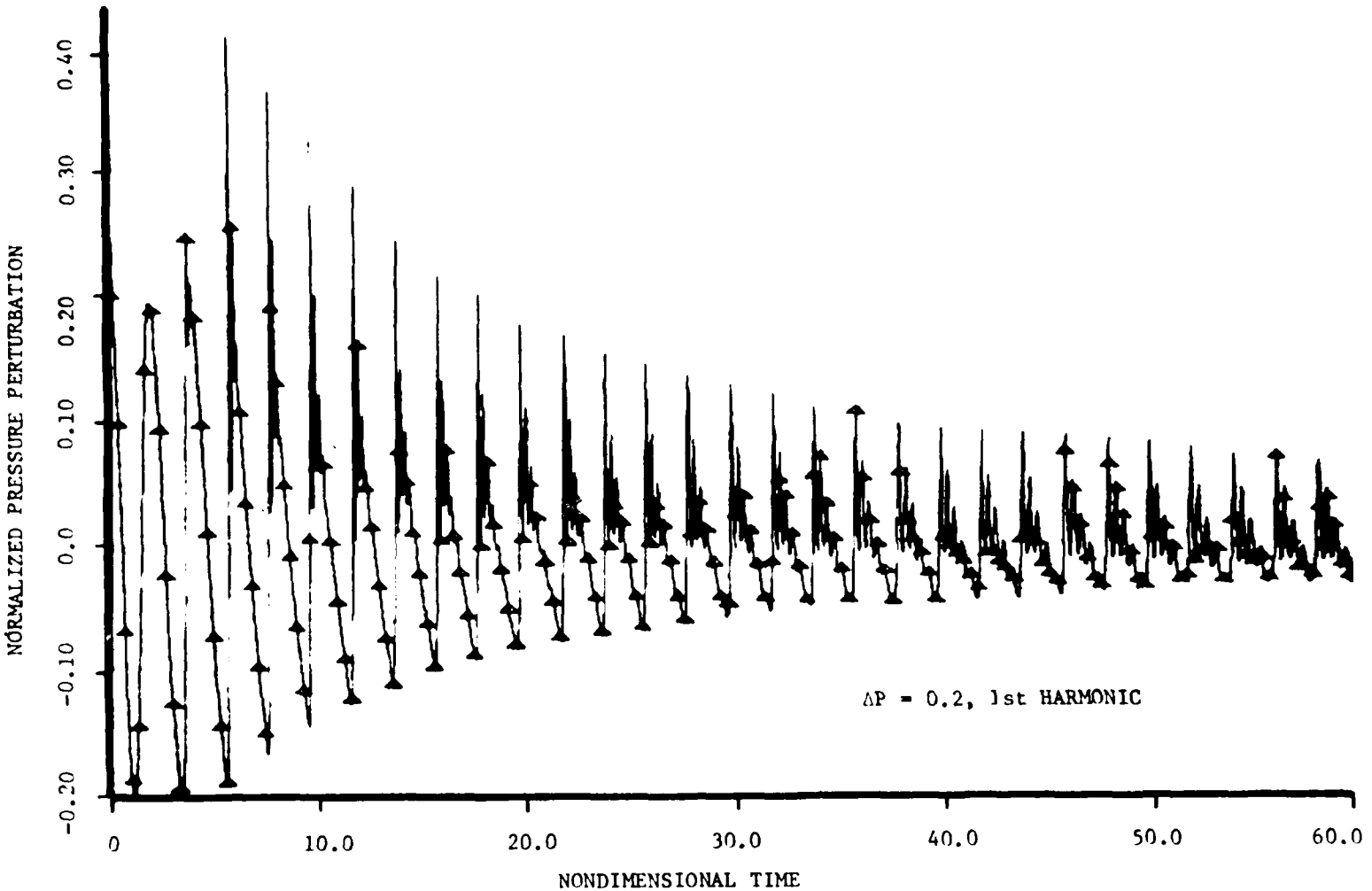

Figure 2.a). Time Evolution of Pressure Oscillations at an End of a Tube (MacCormack).

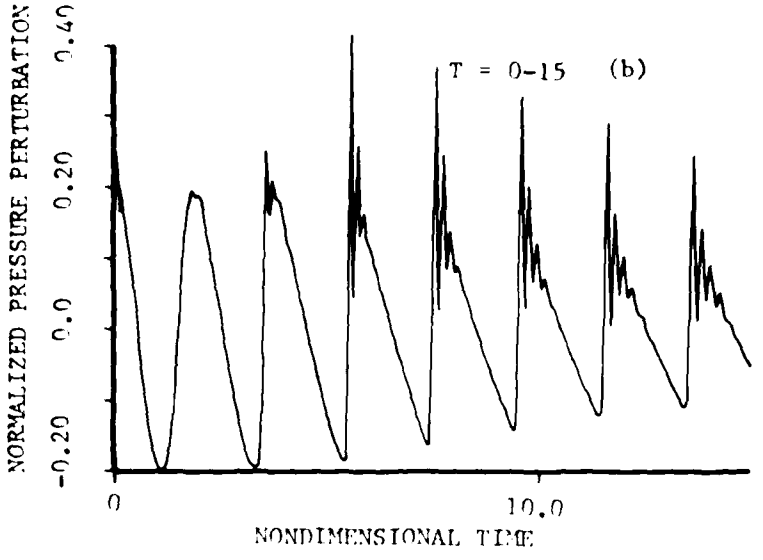

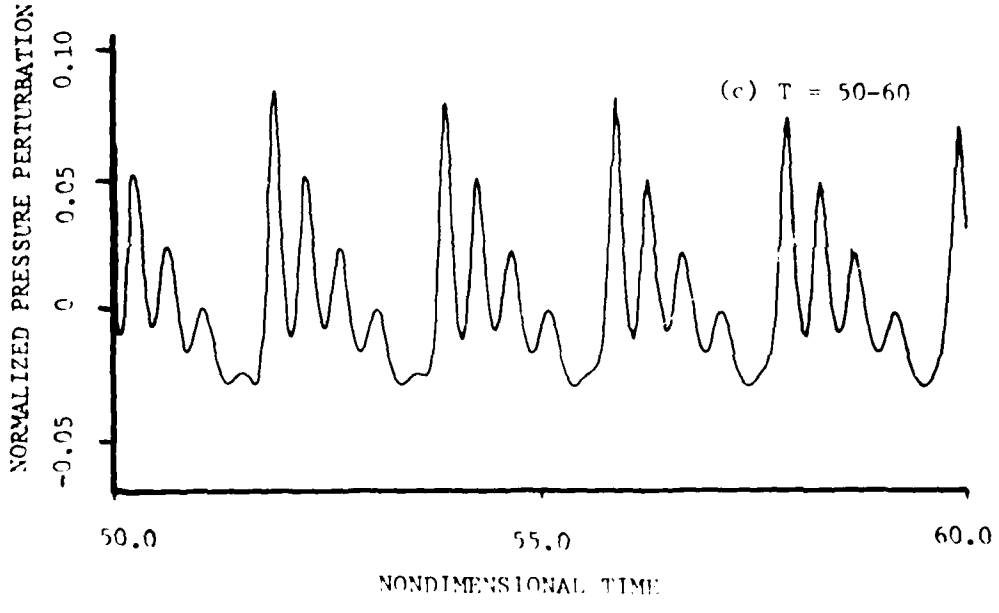

Figure 2(b) and (c). Expanded Views of the Time Evolution of the Pressure Oscillations at an End of a Tube (MacCormack).

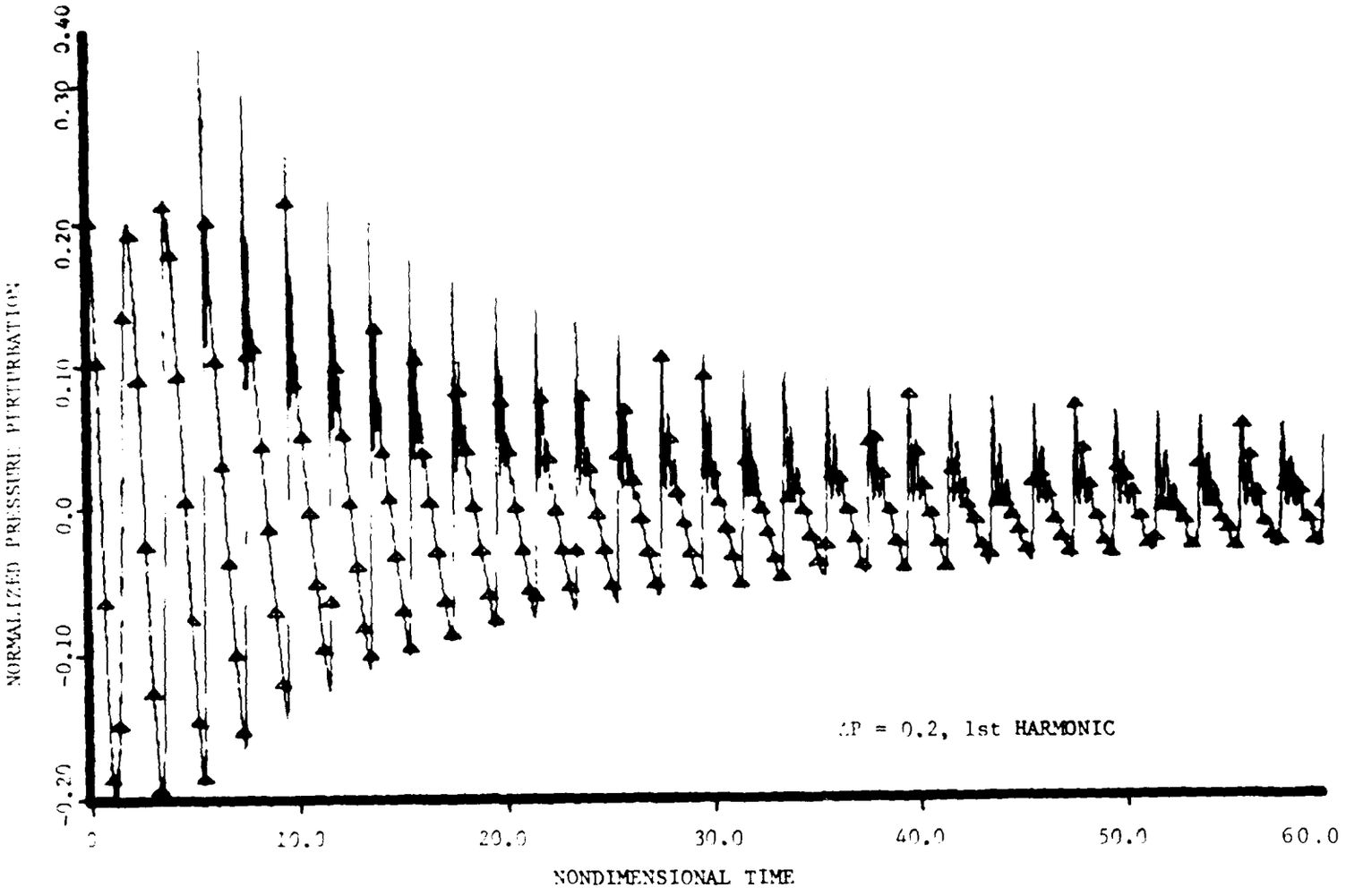

Figure 3 a . Time Evolution of Pressure Oscillations at an End of a Tube (Rubin and Burstein).

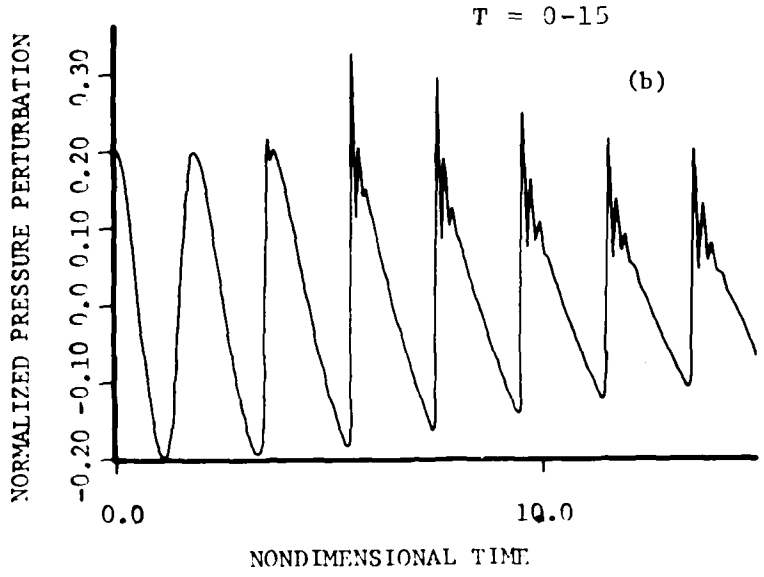

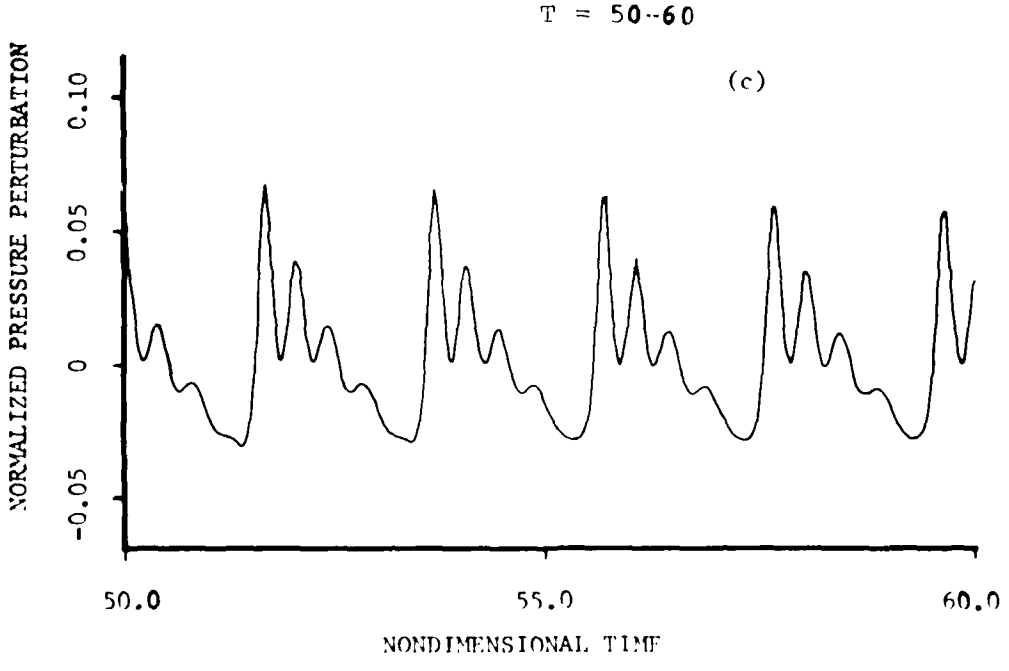

Figure 3(b) and (c). Expanded Views of the Time Evolution of Pressure Oscillations at an End of a Tube (Rubin and Burstein).

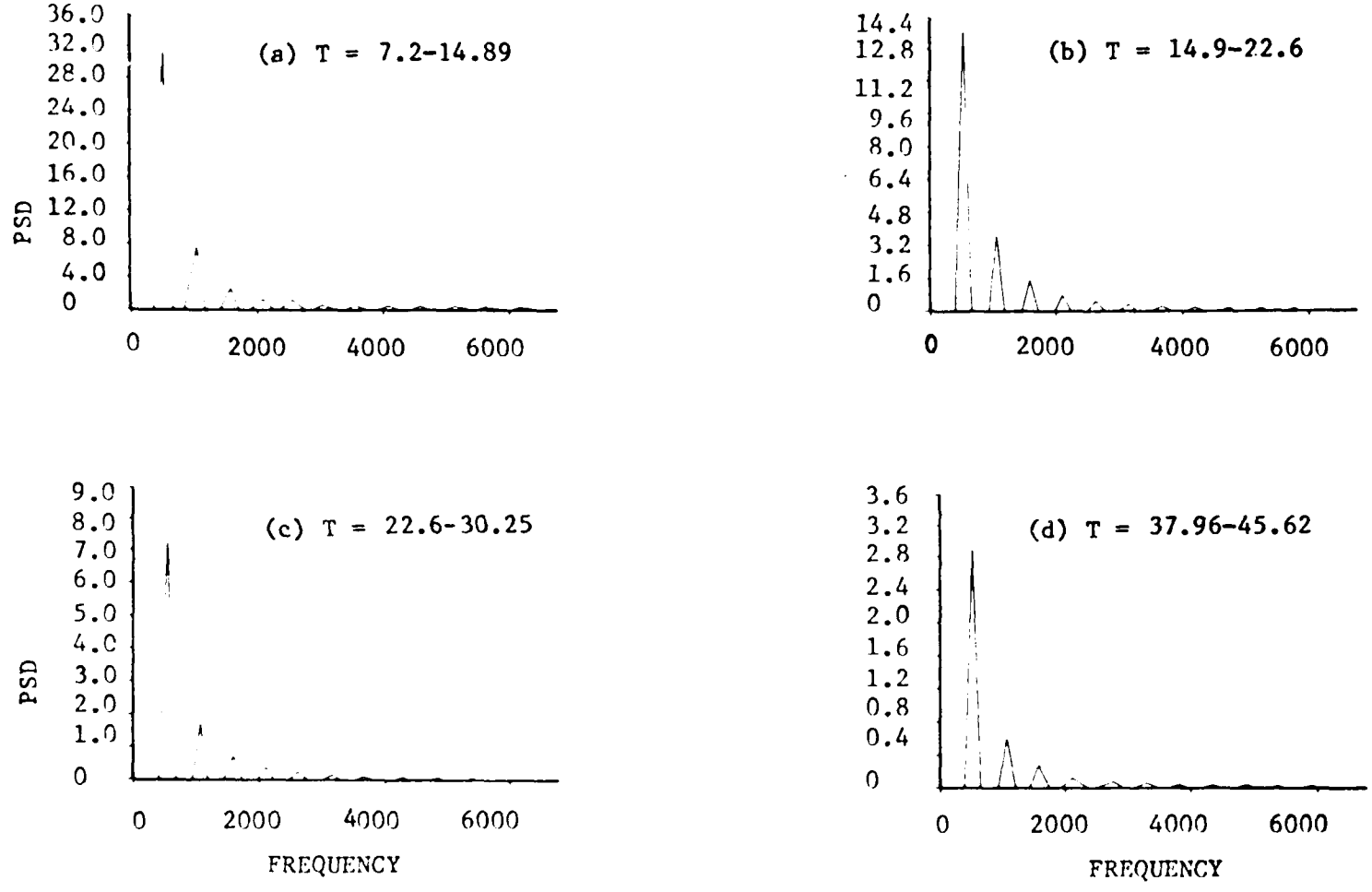

Figure 4.(a) through (d). Time Evolution of Power Spectral Density as a Function of Frequency (LW+H+ACM).

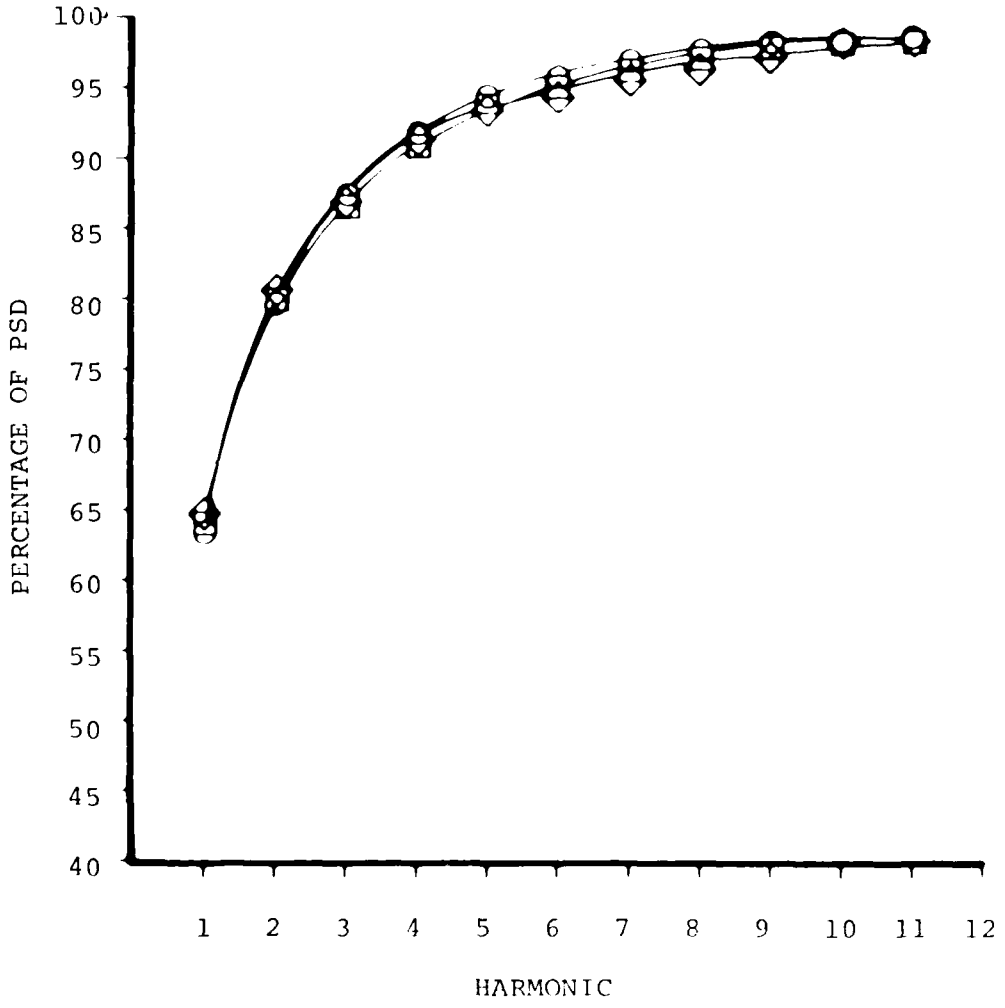

Figure 4(e). Time Evolution of PSD as a Function of Mode Number (LW+H+ACM).

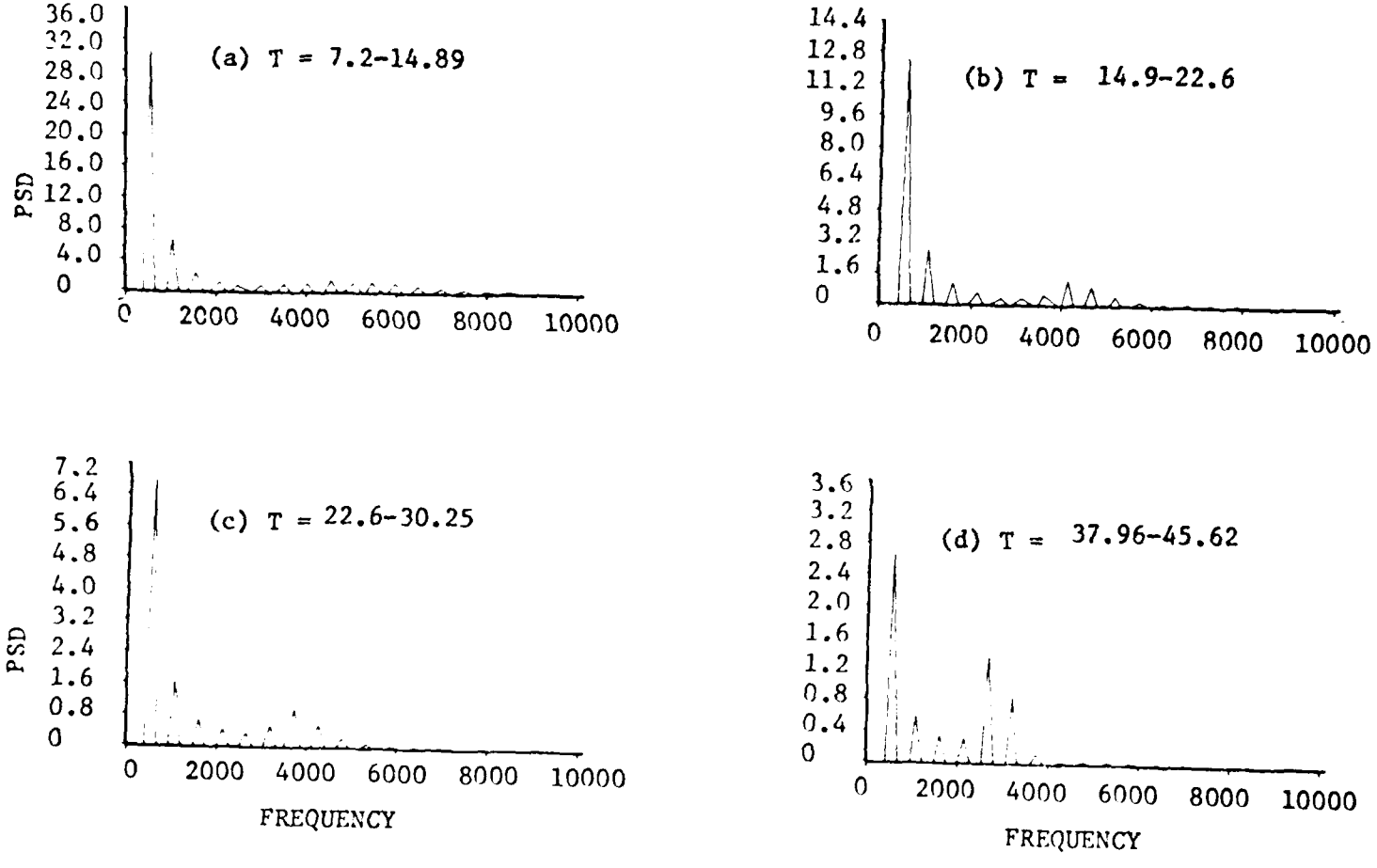

Figure 5(a) through (d). Time Evolution of PSD as a Function of Frequency (MacCormack).

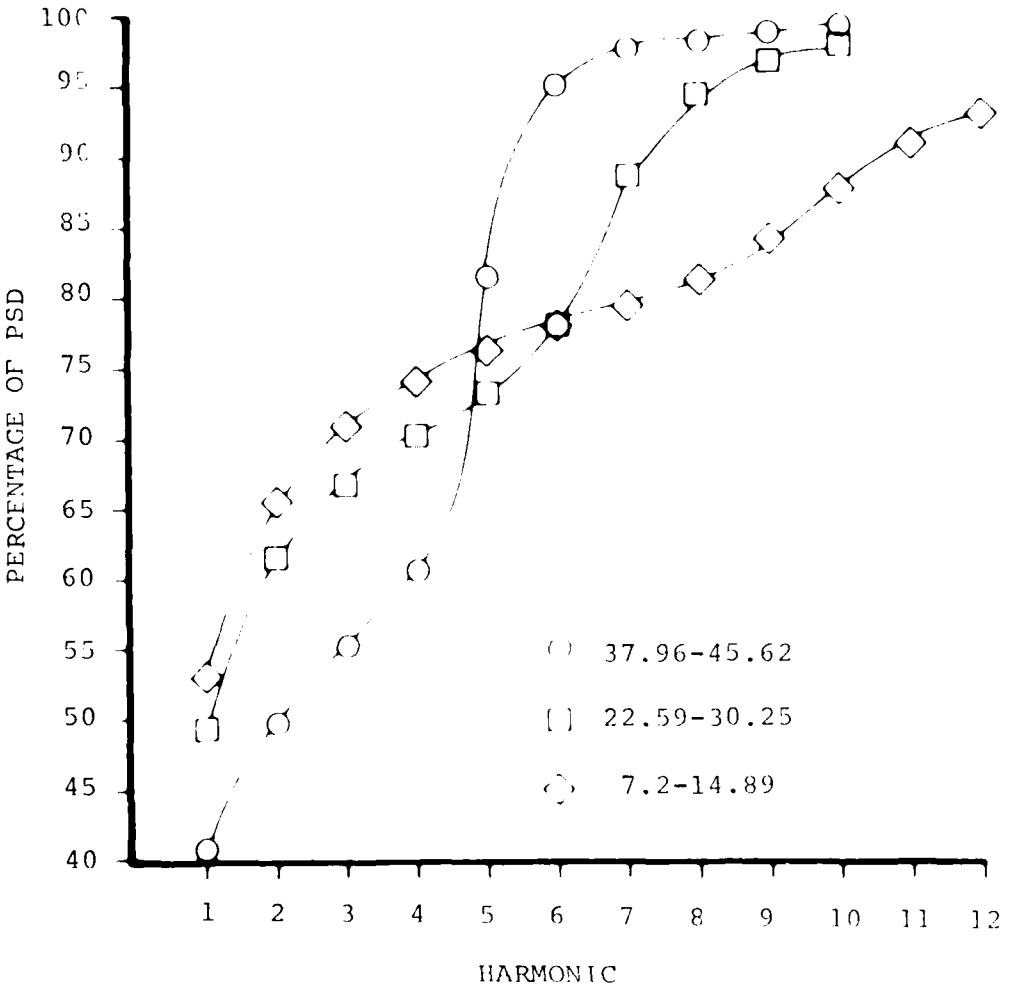

Figure 5(e). Time Evolution of Accumulative PSD as a Function of Mode Number (MacCormack).

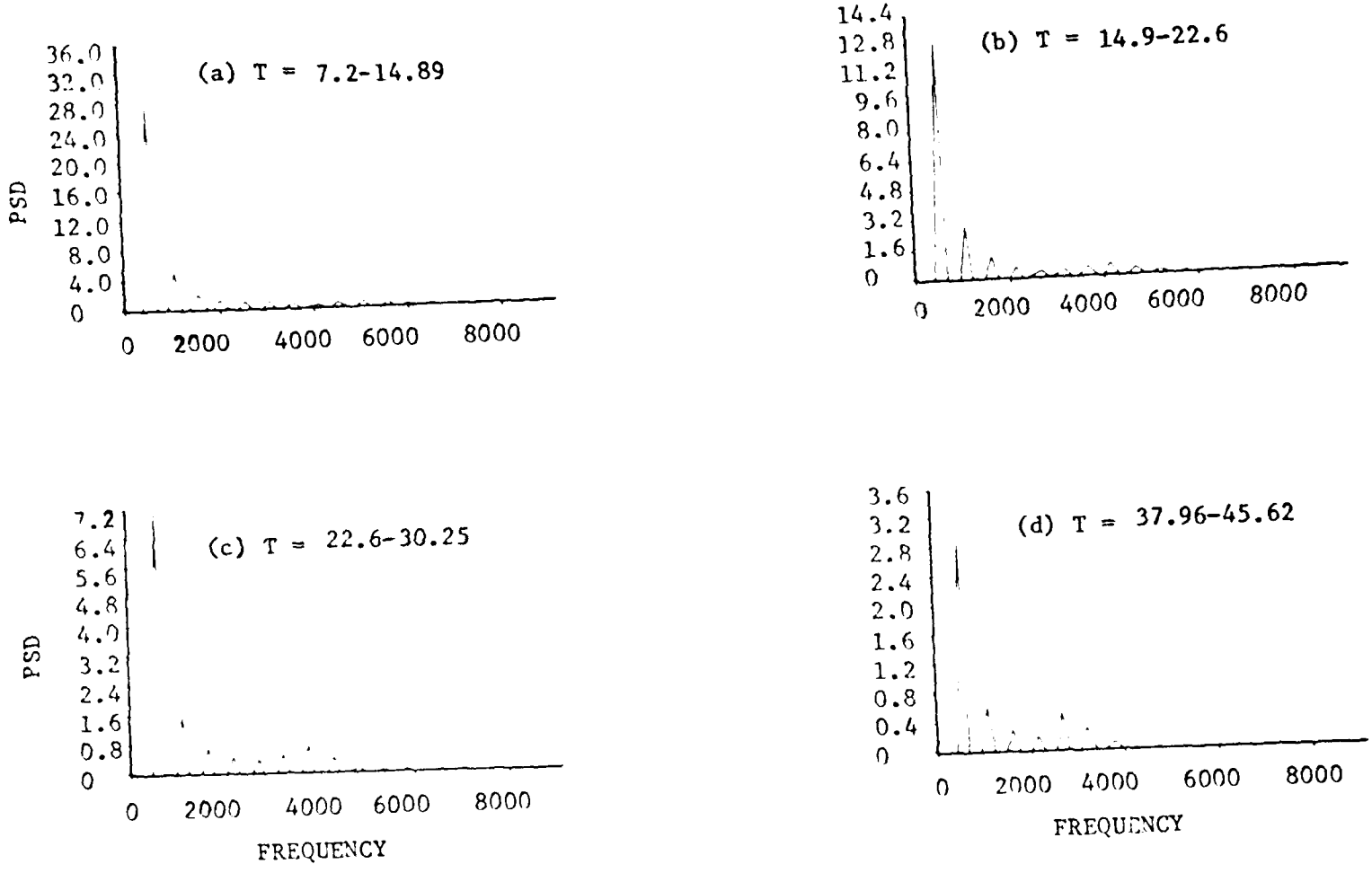

Figure 6(a) through (d). Time Evolution of PSD as a Function of Frequency (Rubin and Burstein).

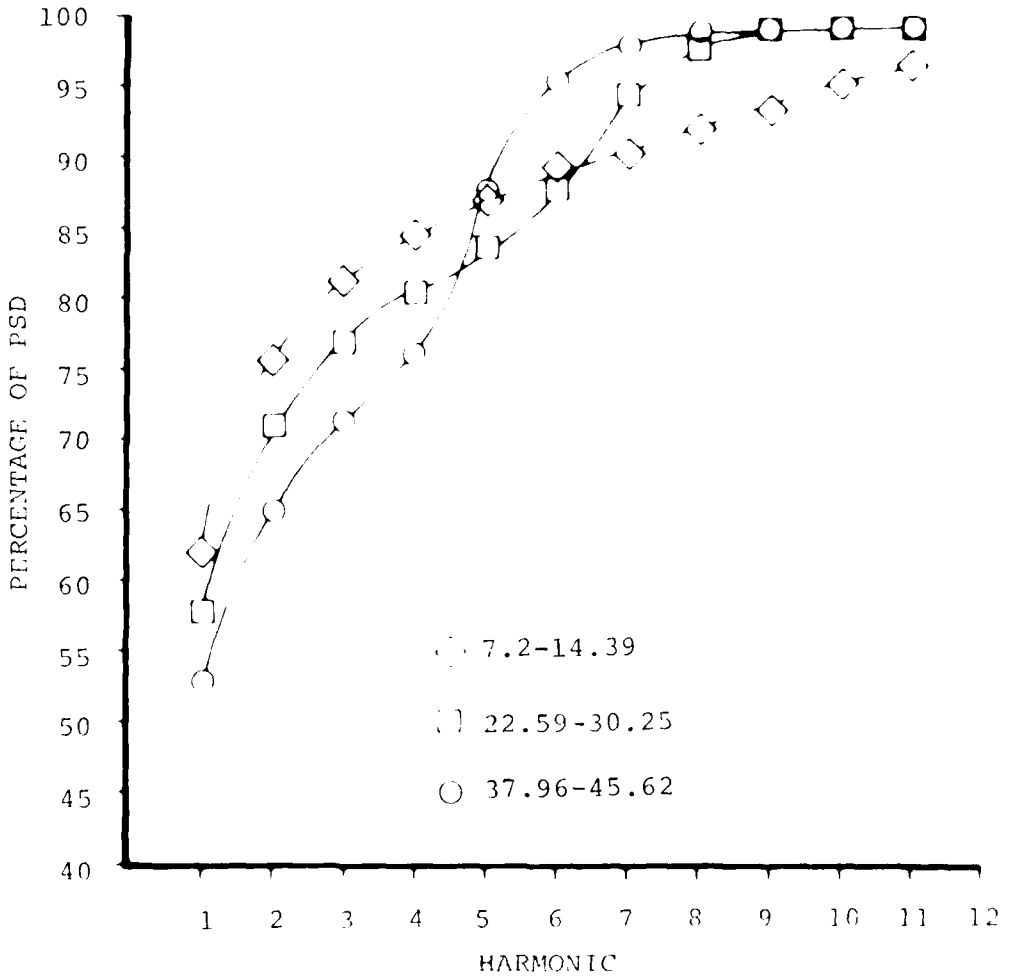

Figure 6(e). Time Evolution of Accumulative PSD as a Function of Mode Number (Rubin and Burstein).

With the LW+II+MCM technique, the initial sine wave disturbance develops into a sharp, triangular, shock-type wave form (Fig. 1). This is the expected result based on the closed form analytical solution to this problem, according to Morse and Ingard.[30] Figures 4a to 4d present the time variation of the power spectral density contained in each mode. These figures indicate that higher modes up to the 11th are excited. Figure 4e shows the time variation of the accumulative power spectral density and indicates that for this numerical scheme there are no erroneous shifts of power spectral density in the high order modes. The acoustic energy distribution varies little with time (once a shock is formed), as expected. The transfer of energy from the fundamental into the higher modes results from the physical process of wave steepening. There is no physical process for transferring energy the other way, i.e, from higher modes into the fundamental.

Figure 2 shows the time evolution of acoustic pressure amplitude at an end of a closed tube when utilizing MacCormack's scheme. An expanded view of the acoustic pressure amplitude between nondimensional times of zero and fifteen is shown in Figure 2b. The development of the initial post shock "wiggle," that appears after the first cycle, into erroneous higher modes is evident. An expanded view of the acoustic pressure amplitude between nondimensional times 50 and 60 (Fig. 2c) shows that the acoustic pressure wave form that at earlier times contained 11-12 harmonics, has now been reduced to a waveform composed of 4-5 harmonics only. The absence of the higher harmonics is evidenced by the discrete humps in the waveform. This trend is also substantiated by the spectral analysis of this solution (shown in Figs. 5a through 5e). Figure 5b indicates an excessively high percentage of acoustic energy in the eighth and ninth harmonics. At the end of the test (after 30 wave cycles), it is shown (Fig. 5d) that this excessively high percentage of acoustic energy has been transferred to the fifth and sixth harmonics. Since, as previously mentioned, there are no known physical processes that can cause such a transition of energy from a higher mode to a lower mode, this phenomenon is apparently a result of numerical error. Figure 5e is another way of demonstrating the same spurious result. Hence, the time variation in the accumulative power spectrum is a result of the dispersive error of the numerical scheme which causes pressure signals to travel at the wrong speed.

The results obtained utilizing the Rubin and Burstein scheme (Figs 3 and 6) are generally similar to the results obtained by utilizing MacCormack's scheme (Figs 2 and 5).

---

30. Morse, P. M. and Ingard, K. V., Theoretical Acoustics, McGraw Hill Book Company, New York, 1968.

A comparison of the results indicates that the first post-shock wiggle appears after the third wave cycle (R-B) compared to the first wave cycle (with MacCormack). Also, the percentage of energy contained in the fundamental mode is greater, and the erroneously high energy in the higher modes is somewhat less with the Rubin and Burstein scheme. In this connection, it should be mentioned that very similar results to those obtained by utilizing the Rubin and Burstein scheme were obtained with the Lax-Wendroff scheme.

The accumulative percentage of power spectral density contained in the respective harmonics for the nondimensional time of 7.2 to 14.89 is shown in Figure 7 for five of the numerical schemes considered. The superiority of the LW+H combination scheme over the standard schemes is evident. The addition of the artificial compression to this combination serves to sharpen shock transitions by exciting higher harmonics that were over damped by the addition of the Hybrid scheme. Thus, compared to the LW and Hybrid result, the LW+H+ACM solution has slightly less energy in the fundamental mode and slightly more energy in the higher harmonics.

All of the earlier methods, i.e., MacCormack, Lax-Wendroff, and Rubin and Burstein were used without adding an artificial viscosity. The effect of an artificial viscosity on the solution was investigated using Hyman's[31] predictor-corrector scheme. Results utilizing this method with two different artificial viscosity coefficients are presented in Figures 8 and 9. The addition of an artificial viscosity to a numerical scheme was conceived as a way to damp post-shock oscillations. Artificial viscosity reduces post shock oscillations at the expense of the higher harmonic components of the waveform. Figure 8 shows what happens when a high value of artificial viscosity is employed (δ equal unity in Hyman's method). In this case the high artificial viscosity prevents a shock from ever forming and the deviations from a perfect sine wave are never large. The results of the spectral analysis of this solution (Figs. 8b and 8c) show the absence of higher harmonic content. Reducing the artificial viscosity coefficient (δ=0.3, the lowest value at which Hyman's method remains stable) yields a much steeper waveform (Fig. 9a), but one whose higher harmonic content is still less than it should be (Figs. 9b and 9c). As time passes, the action of the artificial viscosity continues to damp preferentially the higher harmonics, causing the solution to further degenerate.

---

31. Hyman, James M., "On Robust and Accurate Methods for the Calculation of Compressible Fluid Flows," Part I to be published.

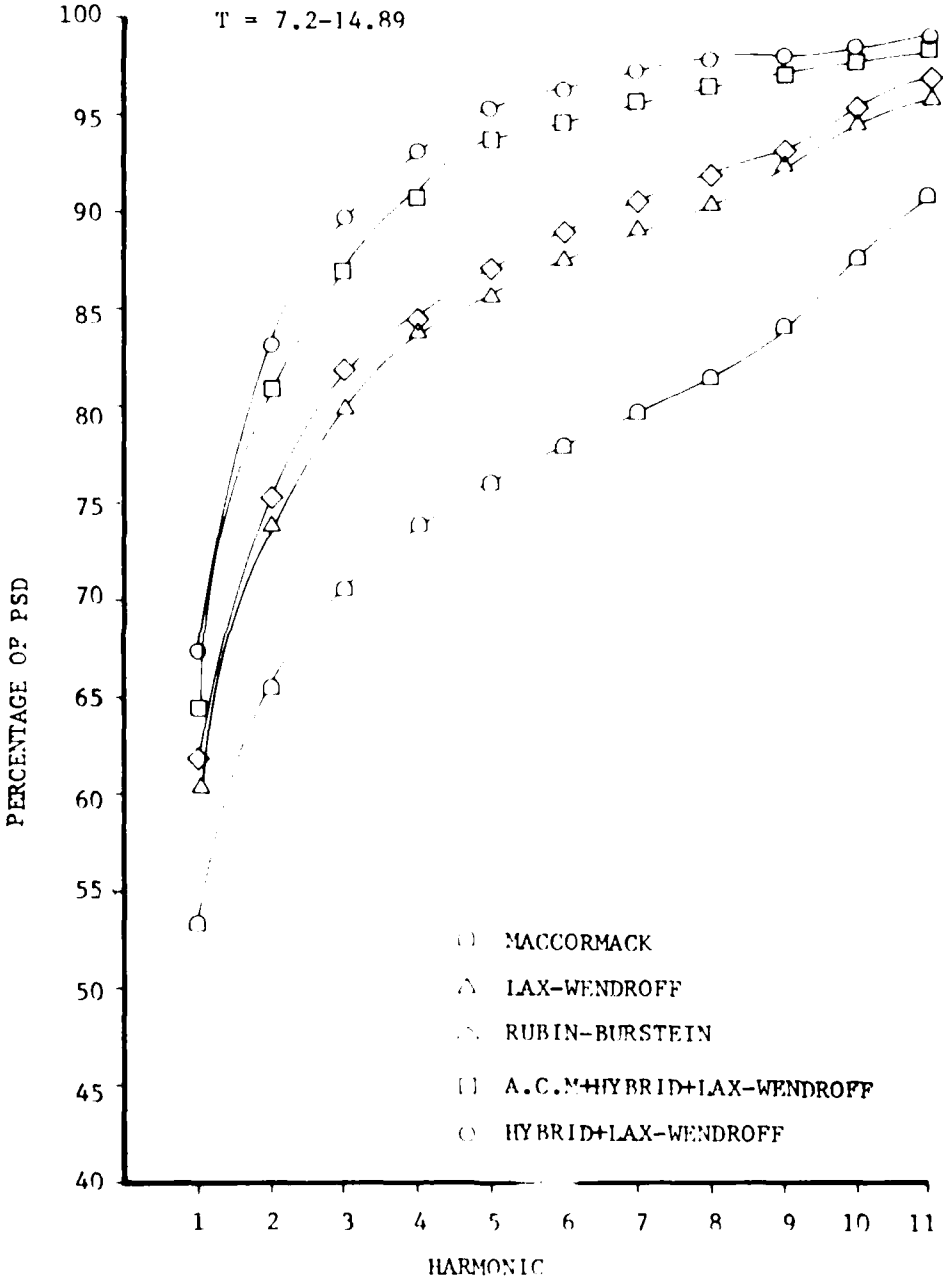

Figure 7. Effect of Finite Difference Scheme on the Accumulative PSD.

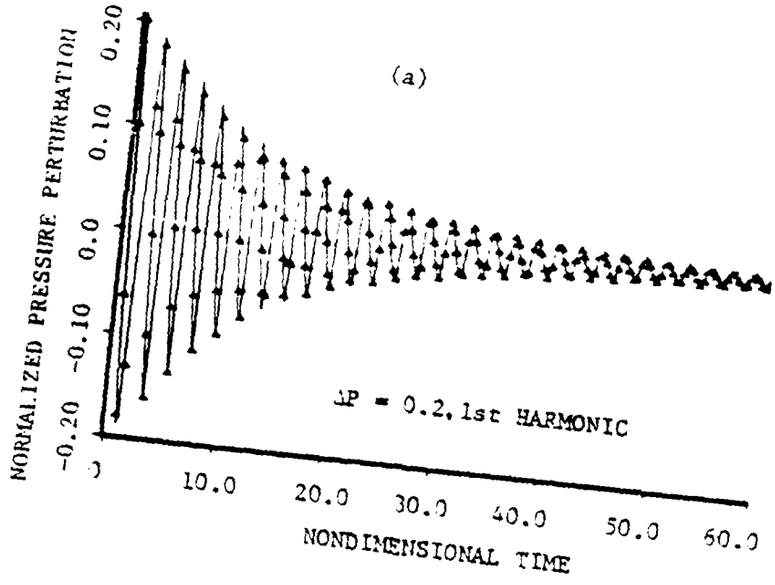

Figure 8(a). Time Evolution of Normalized Pressure Oscillations at an End of a Closed Tube (Hyman's Scheme, $\lambda = 1.0$).

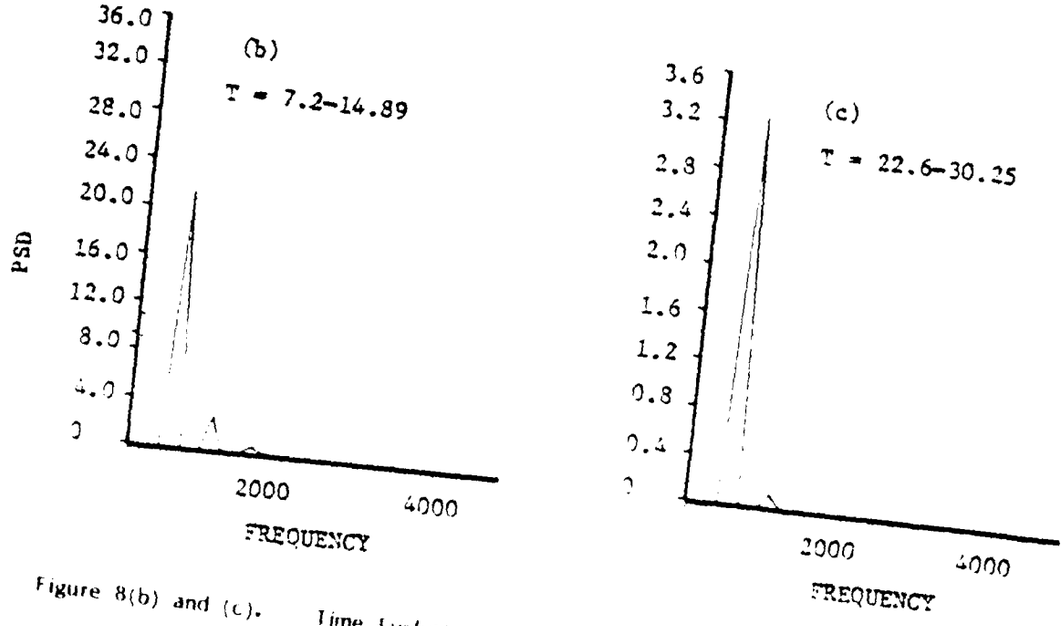

Figure 8(b) and (c). Time Evolution of PSD as a Function of Frequency (Hyman's Scheme, $\lambda = 1.0$).

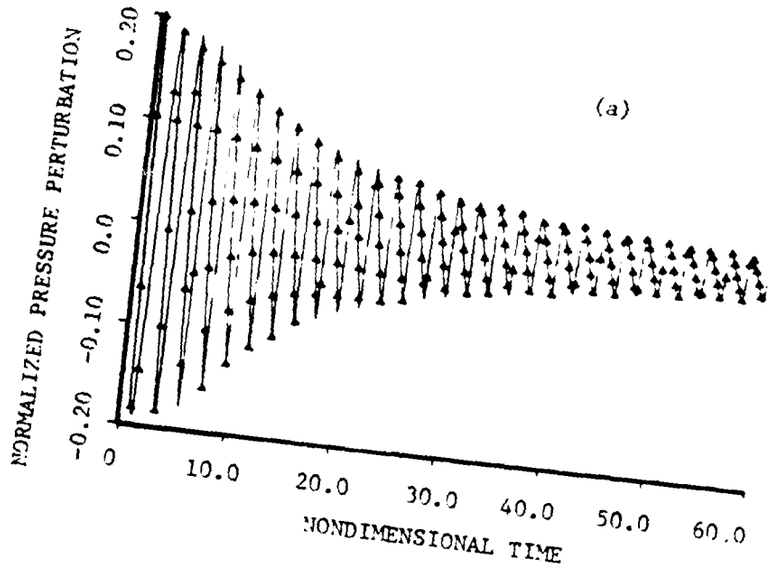

Figure 9(a). Time Evolution of the Normalized Oscillatory Pressure Amplitude at an End of the Closed Tube Utilizing Hyman's Scheme with = 0.3.

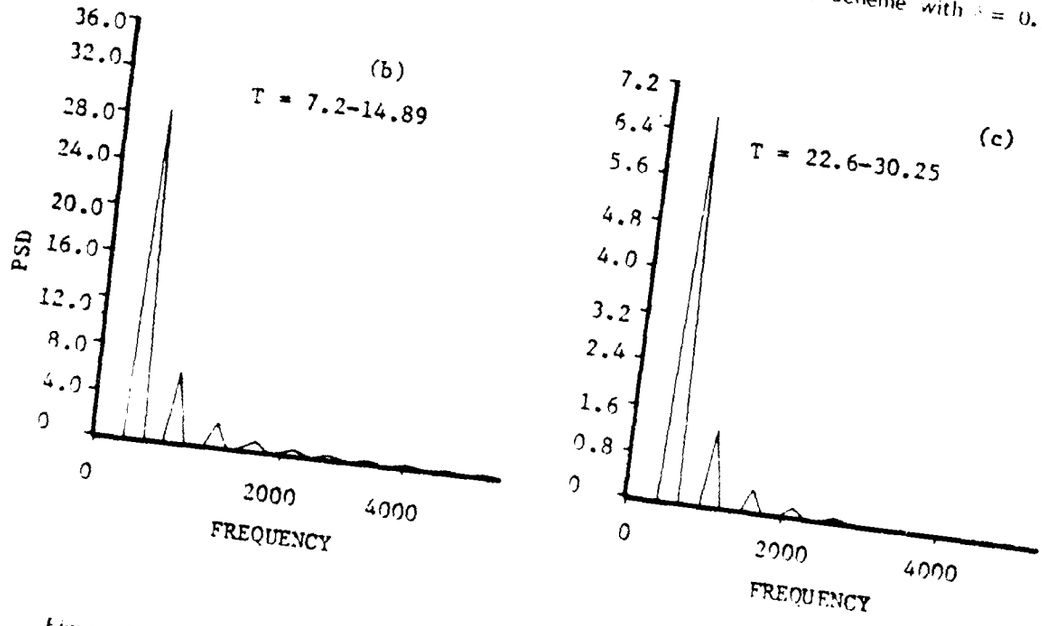

Figure 9(b) and (c). Time Evolution of PSD as a Function of Frequency Utilizing Hyman's Scheme with = 0.3.

As mentioned earlier, artificial viscosity schemes would hamper efforts to determine the actual damping of gas phase oscillations in metalized solid propellants. To illustrate the similarity between the effects of particles and artificial viscosity, the previously described closed end tube problem was modified by the addition of 2% (particle to gas weight flow ratio) of 5 micron particles. The computed results, obtained with the Kuhn and Burstein scheme, are shown in Figure 10. Comparing Figure 10 to Figure 3 shows that the initial post-shock wiggles (Fig. 10b is an expanded view) did not develop into discrete humps in the waveform. As expected, the spectral analysis for the particle case did not show the high erroneous spectral content in the higher harmonics. With particles present, the damping of the high-frequency content of the waveform is due to a real physical process. This is in contrast to the similar, but nonphysical, action of an artificial viscosity.

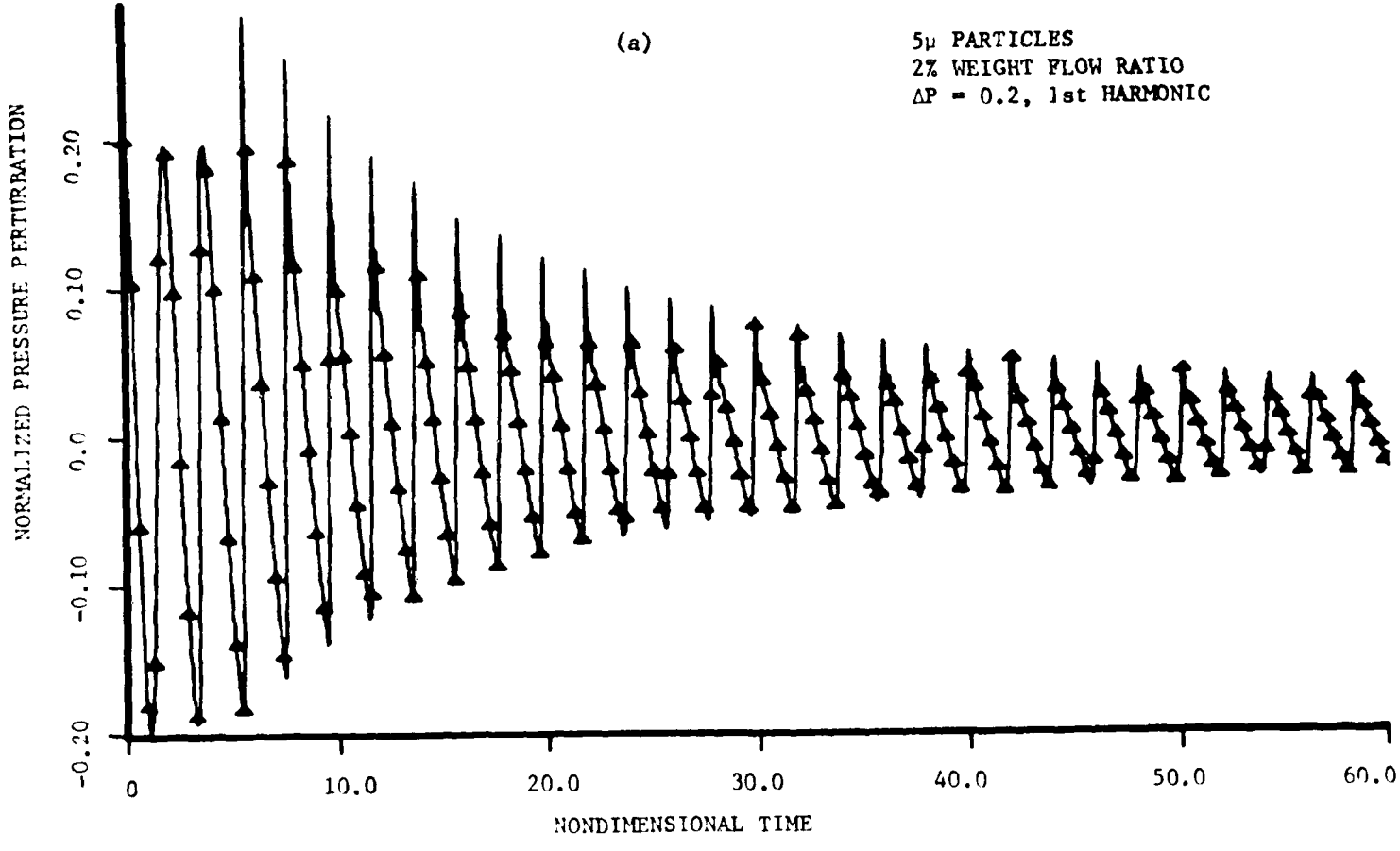

Figure 10(a). Time Evolution of the Normalized Oscillatory Pressure at an End of a Closed Tube Filled with Particles (Rubin and Burstein Scheme).

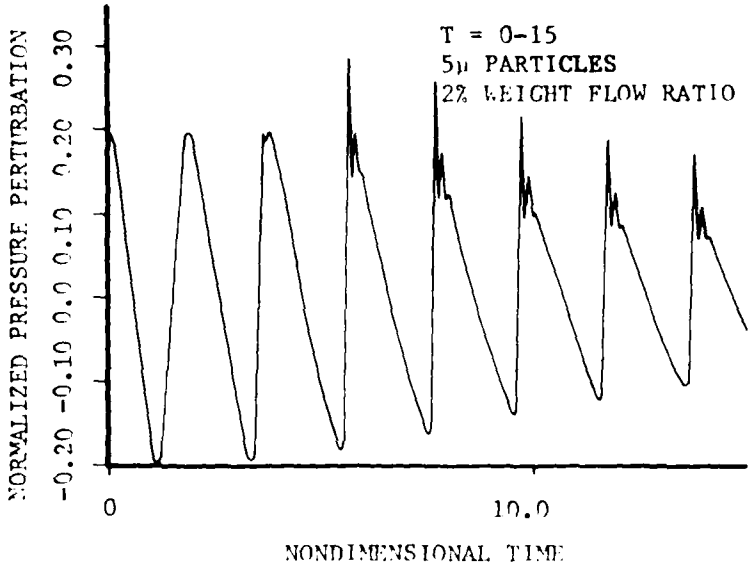

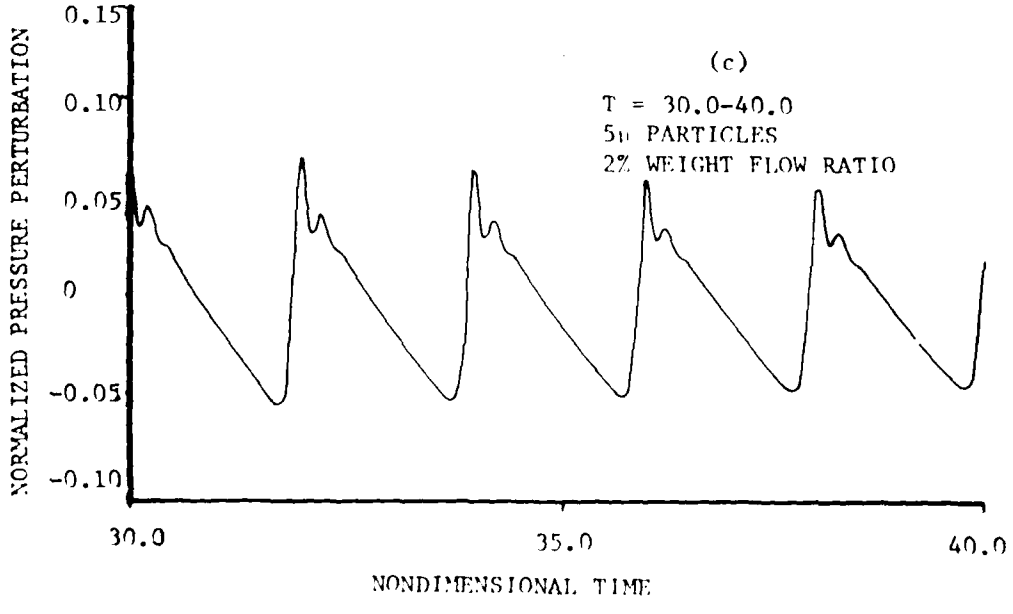

Figure 10(b) and (c). Expanded Views of the Normalized Oscillatory Pressure Amplitude at an End of the Closed Tube Filled with particles (Rubin and Burstein Scheme).

SECTION 3

MOTOR SOLUTIONS

The test problem solutions were used to rank the various methods according to the previously mentioned criteria. It was concluded that the Lax-Wendroff + hybrid + artificial Compression scheme yielded the best results, thus, this scheme was incorporated into the nonlinear instability program described by Levine and Culick.[32]

The quasi-one-dimensional, two-phase, equations of motion to be solved, are shown in Figure 11 in conservative form. The propellant properties and motor geometry (cylindrically perforated grain 59.7cm(23.5 inches long) were taken from Levine and Culick[33] to facilitate comparison with the earlier results. Before presenting the results of the motor solutions, it should be mentioned that, for the motor, propellant and operating conditions utilized, a linear stability analysis shows the fundamental mode to be unstable, while all of the higher modes are stable. It should also be pointed out that at the present time velocity coupling effects are not included in the nonlinear instability program.

Figure 12a shows the pressure time history at the head end of the motor calculated using the LW+H+ACM scheme and an initial first mode disturbance amplitude of 0.4 of the mean pressure. The early history from t = 0 to 15 (nondimensional time) is shown in expanded form in Figure 12b. The initially sinusoidal wave is seen to almost immediately undergo transition to a sharp, oscillation free, shock-type waveform. Figure 12c shows the pressure histories both at the head end and center of the motor for the time interval t = 30 to 60. In this time interval, the wave reaches a limiting amplitude. Examination of the phase differences between the pressure at different locations indicates that the solution is neither a standing wave, nor a traveling wave, but a combination of both.

The same problem was solved using the Gabutti and Sarstedt scheme, the method employed in the original program by Levine and Culick.[34] Figures 13a, b, and c show the head end pressure history and illustrate the development of the initial post-shock wiggle into an erroneous second mode oscillation.

32. Levine and Culick, Op. cit.

33. Ibid.

34. Ibid.

GAS EQUATIONS IN CONSERVATIVE FORM

CONTINUITY:
$$\frac{\partial \rho}{\partial t} + \frac{1}{A}\frac{\partial}{\partial x}(\rho u A) = \omega$$

MOMENTUM:
$$\frac{\partial(\rho u)}{\partial t} + \frac{1}{A}\frac{\partial}{\partial x}\left[(p + \rho u^2)A\right] = \frac{p}{A}\frac{dA}{dx} + u_{s_{ll}}\omega + \sum_l \left[F_{p_l} + \beta_l \omega\left(u_{p_{s_{l_{ll}}}} - u_{p_l}\right)\right]$$

ENERGY:
$$\frac{\partial}{\partial t}\left[\rho\left(\frac{c_p T}{\gamma} + \frac{u^2}{2}\right)\right] + \frac{1}{A}\frac{\partial}{\partial x}\left[\rho u\left(\frac{c_p T}{\gamma} + \frac{u^2}{2}\right)A\right]$$
$$= -\frac{1}{A}\frac{\partial}{\partial x}(upA) + \omega\left(c_p T_s + \frac{u_s^2}{2}\right) + \sum_l \left[Q_{p_l} + u_{p_l} F_{p_l} + \beta_l \omega\left[c_s\left(T_{p_{s_l}} - T_{p_l}\right) + \frac{1}{2}\left(u^2_{p_{s_l}} - u^2_{p_l}\right)\right]\right]$$

PARTICLE EQUATIONS IN NONCONSERVATIVE FORM

CONTINUITY:
$$\frac{\partial \rho_{p_l}}{\partial t} + \frac{1}{A}\frac{\partial}{\partial x}(\rho_{p_l} u_{p_l} A) = \beta_l \omega$$

MOMENTUM:
$$\frac{\partial u_{p_l}}{\partial t} + u_{p_l}\frac{\partial u_{p_l}}{\partial x} = -\frac{F_{p_l}}{\rho_{p_l}}$$

ENERGY:
$$\frac{\partial T_{p_l}}{\partial t} + u_{p_l}\frac{\partial T_{p_l}}{\partial x} = -\frac{Q_{p_l}}{\rho_{p_l} c_s}$$

Figure 11. Two-Phase Equations of Motion.

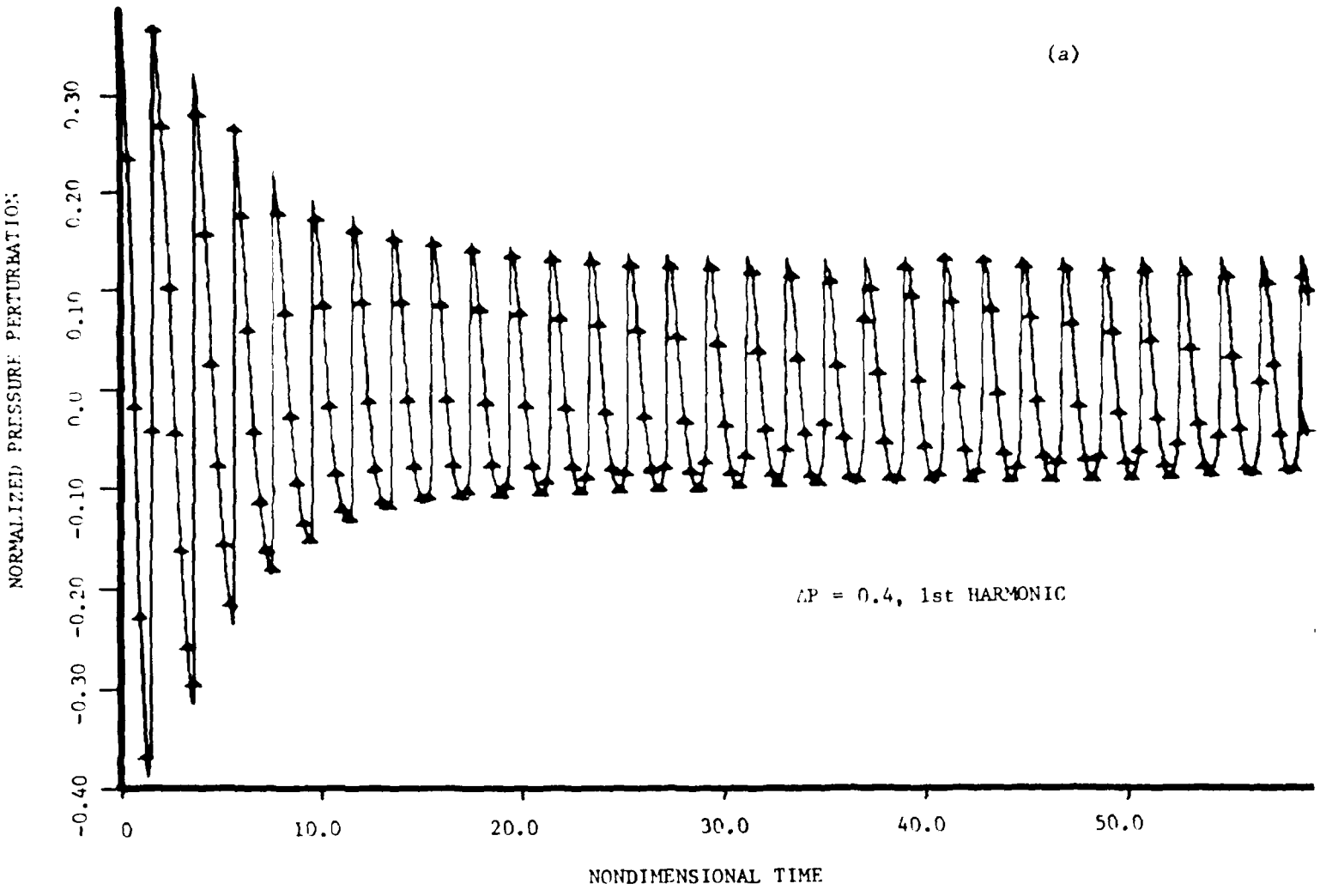

Figure 12.a. Time History of the Normalized Oscillatory Amplitude at the Head of the Motor (A+H+N-4).

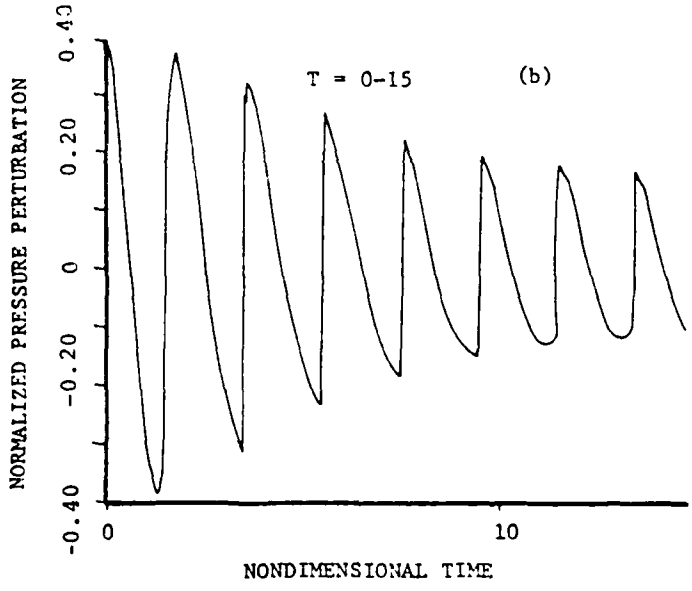

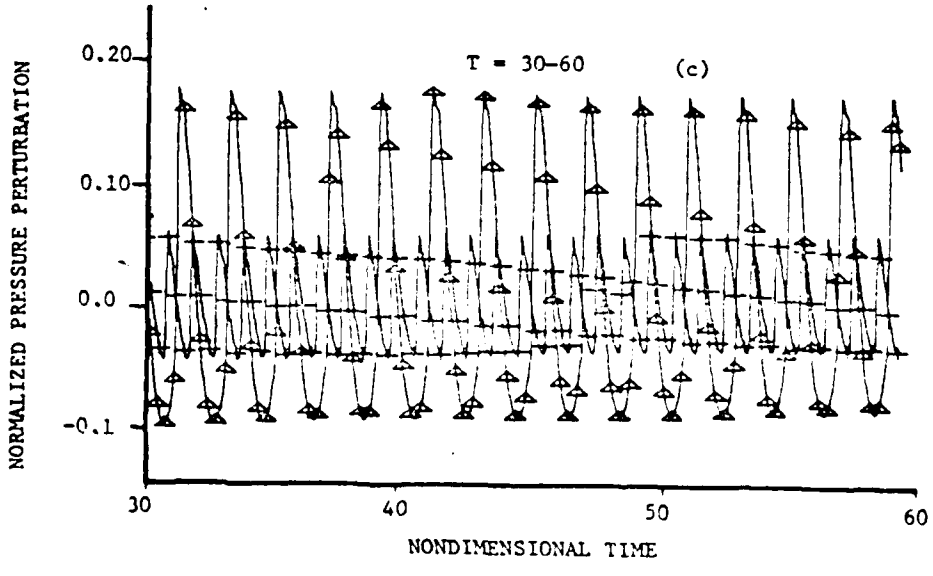

Figure 12 (b) and (c). Expanded Views of the Time Evolution of the Normalized Oscillatory Pressure Amplitude at the Head End of the Motor, 1st Harmonic, Standing Wave, $\Delta P = 0.4$ (DW+IH+ACM).

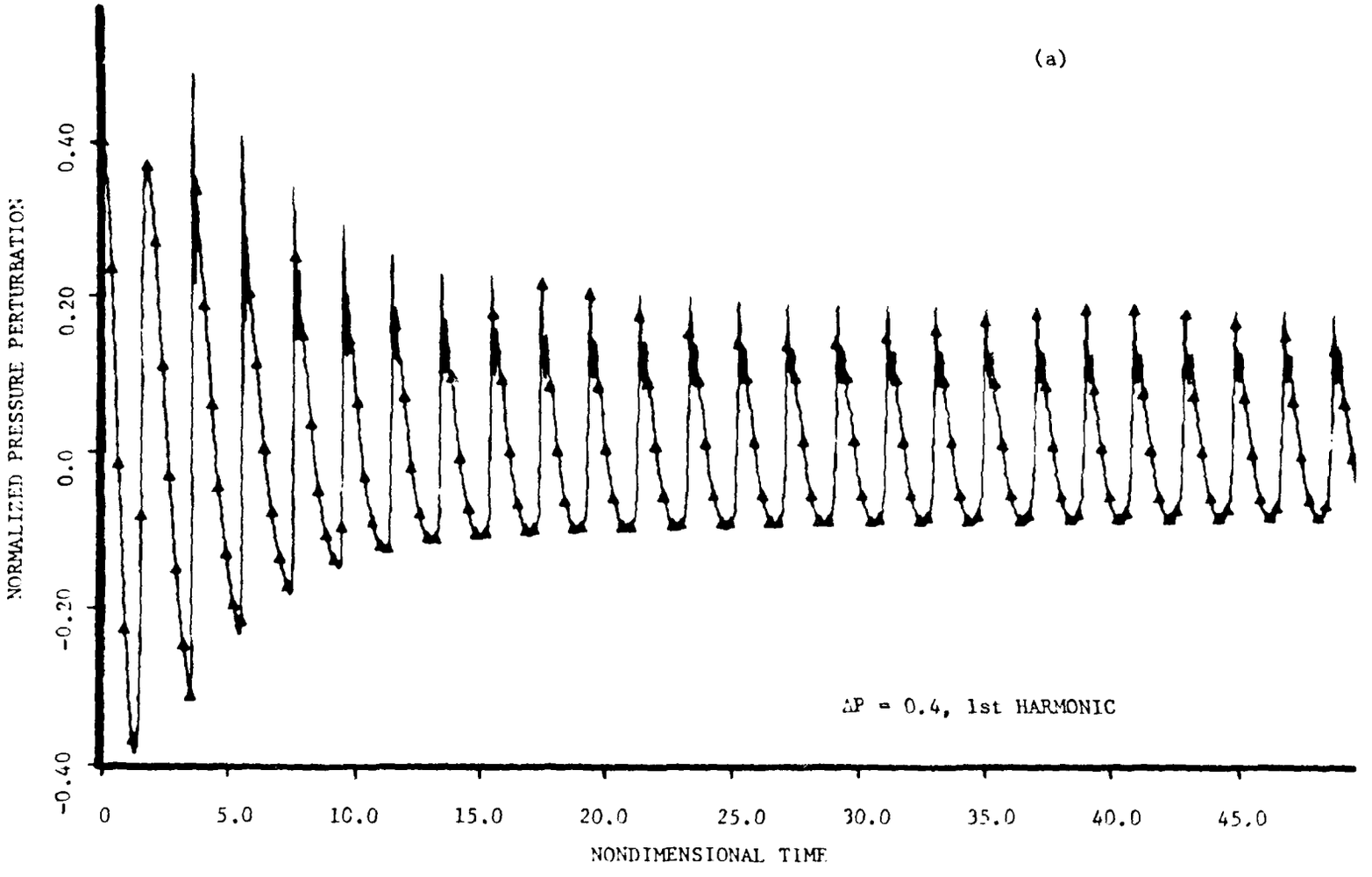

Figure 13(a). Time Evolution of the Normalized Oscillatory Pressure Amplitude at the Head End of the Motor (Rubin and Burstein Scheme).

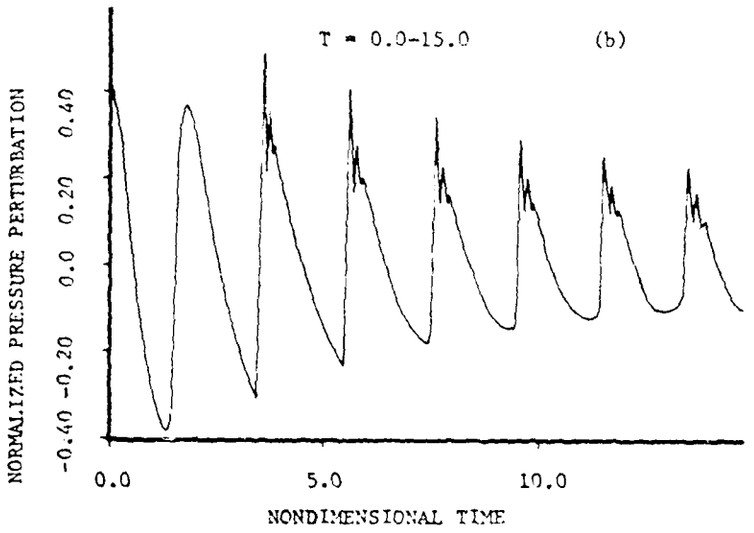

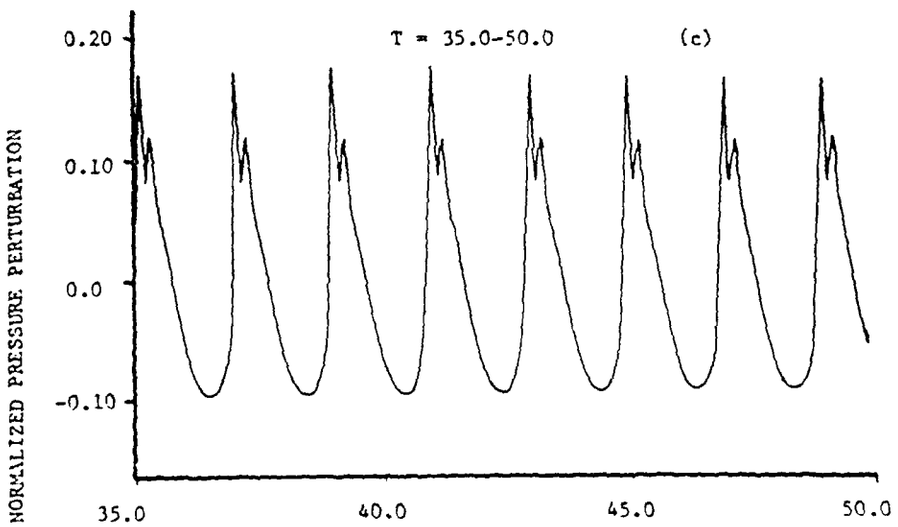

Figure 13(b) and (c). Expanded Views of the Time Evolution of Normalized Oscillatory Pressure Amplitude at the Head End of the Motor, 1st Harmonic, Standing Wave, (Rubin and Burstein Scheme).

The marked improvement obtained with the new solution scheme for this severe test case was gratifying.

To examine the effect of initial disturbance amplitude, the same problem was solved using the LW+II+ACM scheme and initial first mode disturbance amplitudes of 0.2 and 0.05 of the mean pressure. The head end pressure histories for these cases are shown in Figures 14 and 15 respectively. In all three cases, 0.4, 0.2, and 0.05 initial amplitude shown in Figures 12, 14, and 15 respectively, the solution reaches the same limiting amplitude of about 0.12 of the mean pressure. This result was quite surprising in view of the results by Levine and Culick[35] which demonstrated a strong effect of initial disturbance on limiting amplitude. The explanation appears to lie in the fact that the present solutions were for gas only, while the earlier solutions were for the same motor, operating conditions, and propellant, but with 15% aluminum added (0.36 particle gas weight flow ratio). Hence, it seems that nonlinear particle damping effects play a critical role in establishing limiting amplitude.

The spectral analysis results corresponding to the 0.05 amplitude case are shown in Figures 16a through 16d. These results clearly demonstrate the excitation of higher harmonics as the original disturbance grows and steepens.

An important application of nonlinear instability analysis is the prediction of motor response to pulse type disturbances. The Levine and Culick[36] nonlinear instability program has a limited ability to generate pulse type waveforms (it will be expanded soon). This capability was used to test the ability of the LW+II+ACM method to treat such problems. The results of two solutions will be discussed. In both cases, the initial pressure disturbance waveform was taken to be of the form $\sin^6(\pi X/\ell)$ with an amplitude equal to 0.4 of the mean pressure. This produces the centered, symmetric waveform shown in Figure 17. The difference between the two cases was the initial velocity at t = 0. In one case, the velocity was taken to be $\Delta P/\gamma$, while in the second case, the velocity (nondimensional) was taken to be zero. The first case represents a traveling pulse. The value of velocity is taken such that the initial pulse represents a right traveling wave.* The second case corresponds to a "standing" pulse. The pulse propagates as the sum of equal left and right traveling waves, each having half the initial amplitude.

---

35. Ibid.

36. Ibid.

*Actually setting $\Delta V = \Delta P/\gamma$ only produces a pure and right traveling wave in the linear limit as ΔP approaches 0.

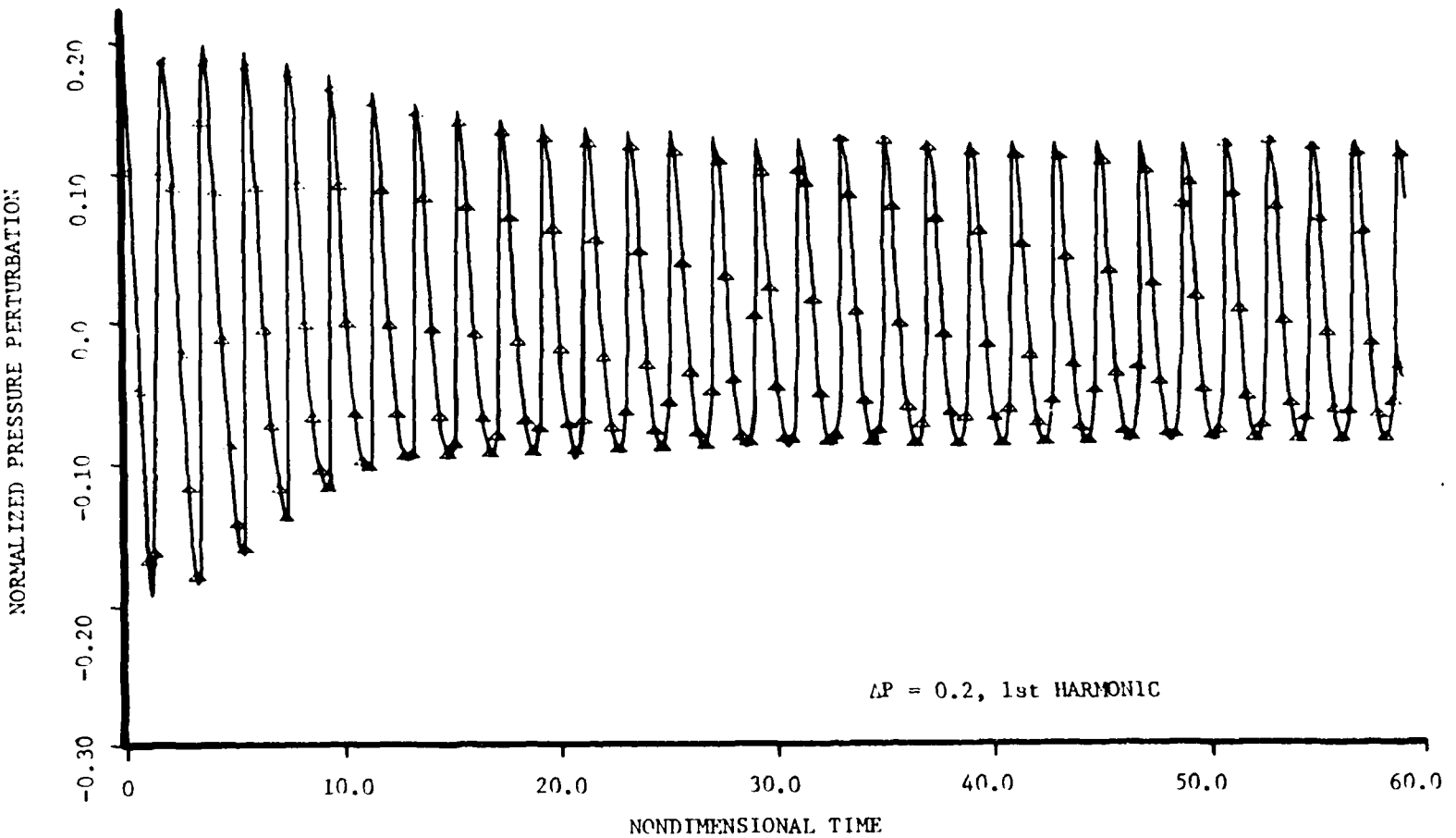

Figure 14. Time Evolution of the Normalized Oscillatory Pressure Amplitude at the Head End of the Motor (CW+H+NOM).

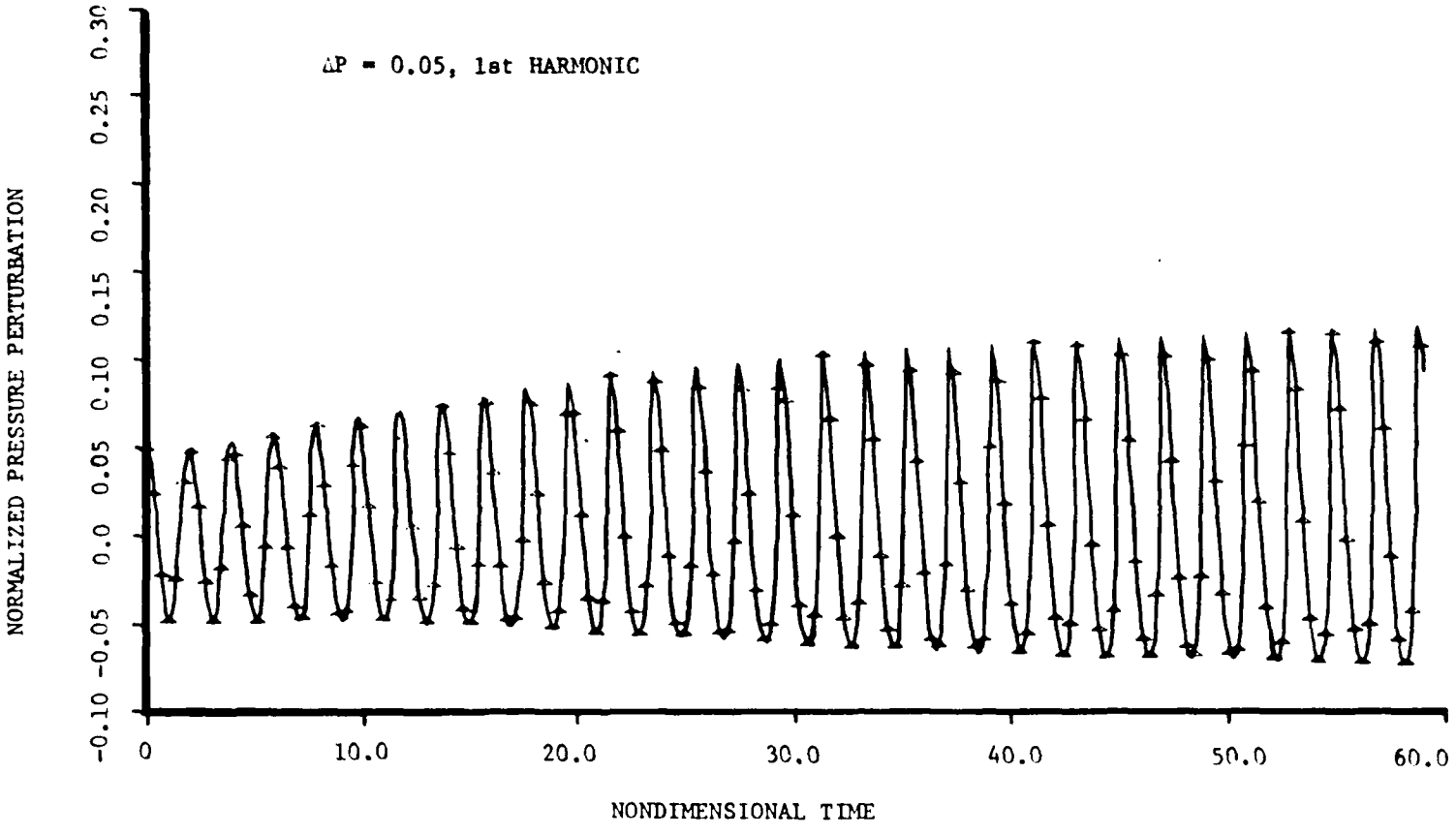

Figure 15. Time Evolution of the Normalized Oscillatory Pressure Amplitude at the Head End of the Motor (LW+H+ACM).

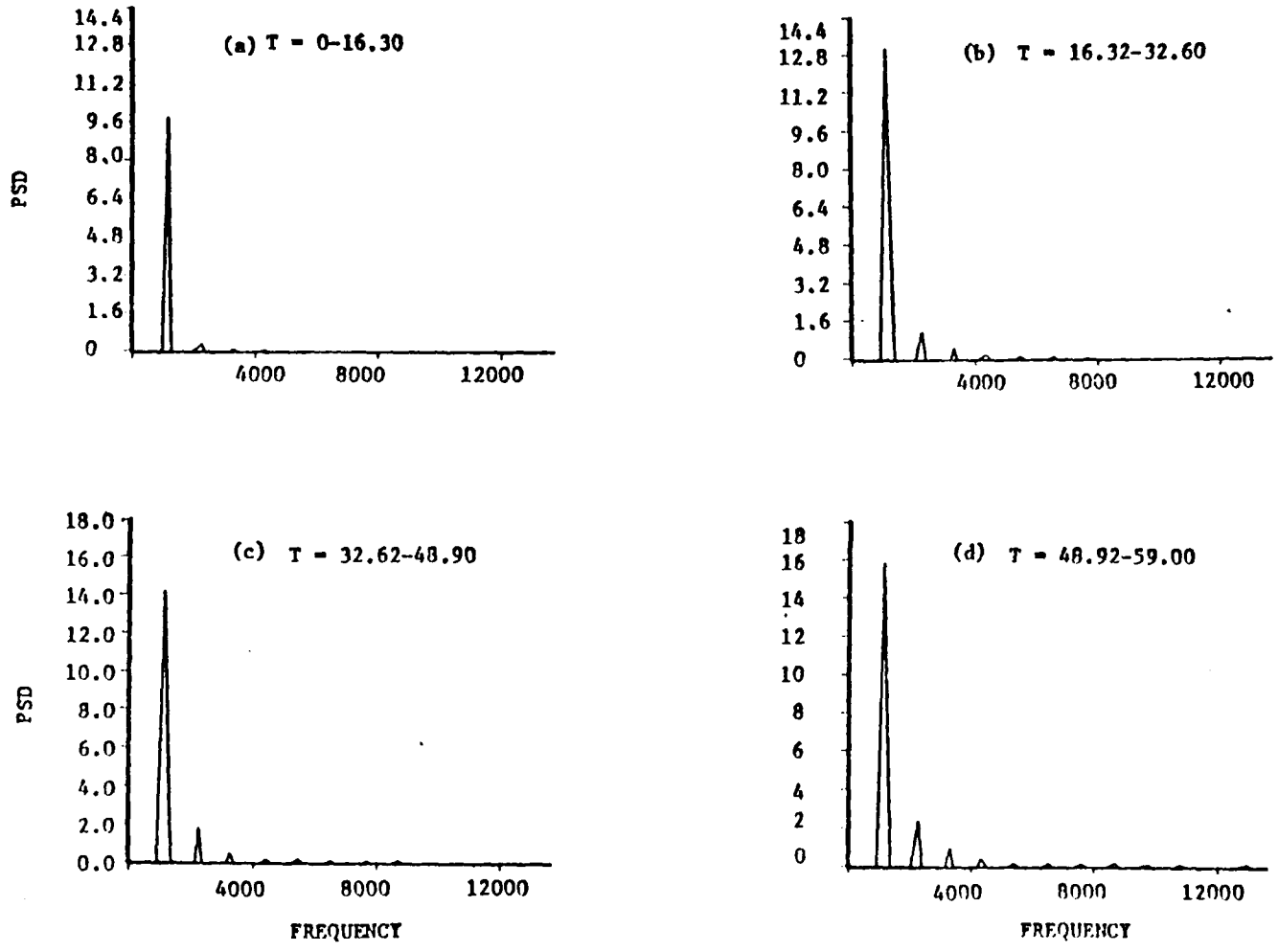

Figure 16 a. through d. Time Evolution of the Power Spectral Density as a Function of Frequency, 1st Harmonic, Standing Wave, $\Delta P = 0.05$ [illegible].

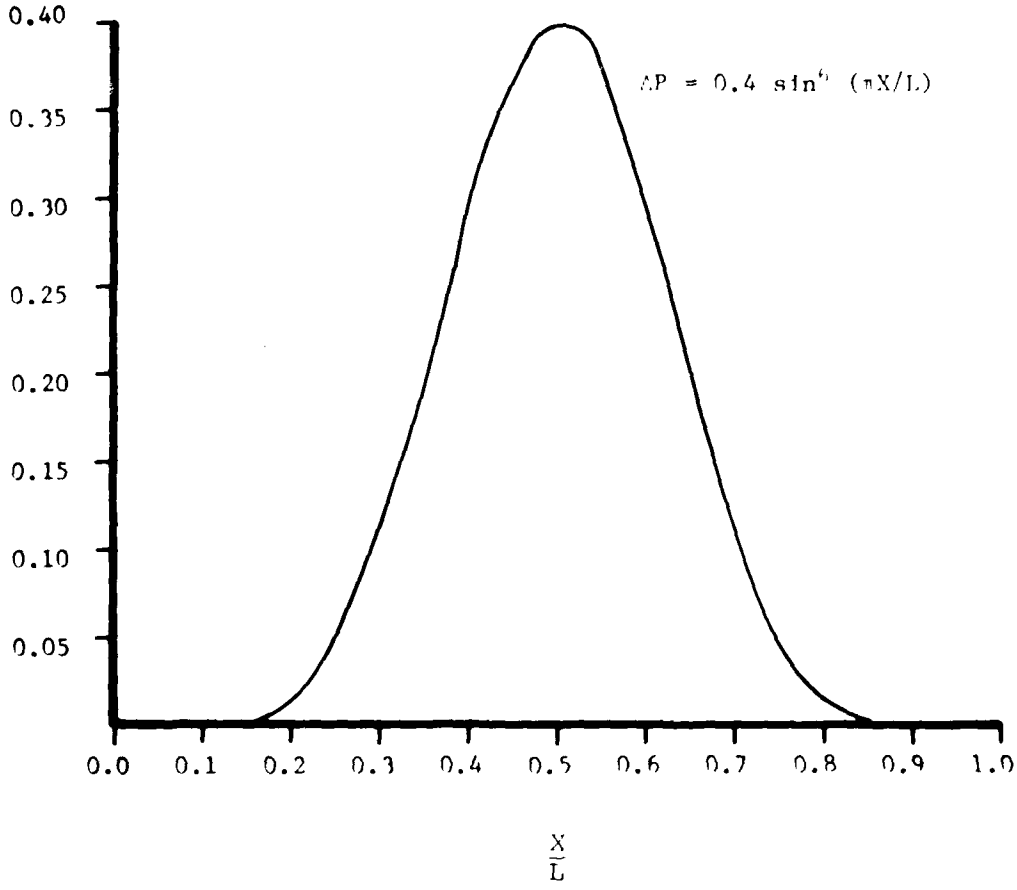

Figure 17. Axial Variation of the Normalized Pressure Amplitude of the Pulse.

The calculated pressure histories at the head end of the motor for each of these disturbances are shown in Figure 18 (traveling) and Figure 19 (standing). The dramatic difference between the results demonstrates the importance of the velocity disturbance associated with a pressure pulse. The traveling pulse is immediately transformed into steep-fronted shock type waveform and decays until it reaches the same limiting amplitude as the solutions started from first mode sinusoidal disturbances. Spectral analyses of this solution for three time intervals are shown in Figures 20a to 20c. At early times (Fig. 20a) the traveling pulse disturbance contained a large percentage of the fundamental, but a significant higher harmonic content is also evident. As the limiting amplitude was approached, at later times, the percentage of energy in the fundamental increased.

The pressure history of the standing pulse disturbance is shown in Figure 19. The time variation of the waveform is quite complex in this case. The spectral analysis results shown in Figures 21a to 21c help to clarify what is happening. At early times, a symmetric standing pulse centered in the motor contains essentially only even harmonics (Fig. 21a), with the second harmonic dominating. The fundamental and odd harmonics are infinitesimal at this time. Since only the fundamental is unstable for this motor, the even harmonics decay with time, while the fundamental begins to grow. In the time interval from about t = 20 to 40, the waveform becomes complex as it transitions from a steep second dominated wave to an almost sinusoidal wave at the fundamental frequency. Recently, this solution was continued out to a nondimensional time of 180. The wave continues to decay out to a time of about 100. At this time, the wave amplitude is only 1.6% of the mean pressure (compared to 40% initially) and the wave is essentially a pure fundamental sine wave. After t = 100, the wave starts to grow, and is still growing at t = 130. As the wave grows, higher harmonic content again begins to appear as a result of energy transfer from the fundamental. It is expected that the oscillation will continue to grow until it reaches the same limiting amplitude as the other test cases for this motor and propellant.

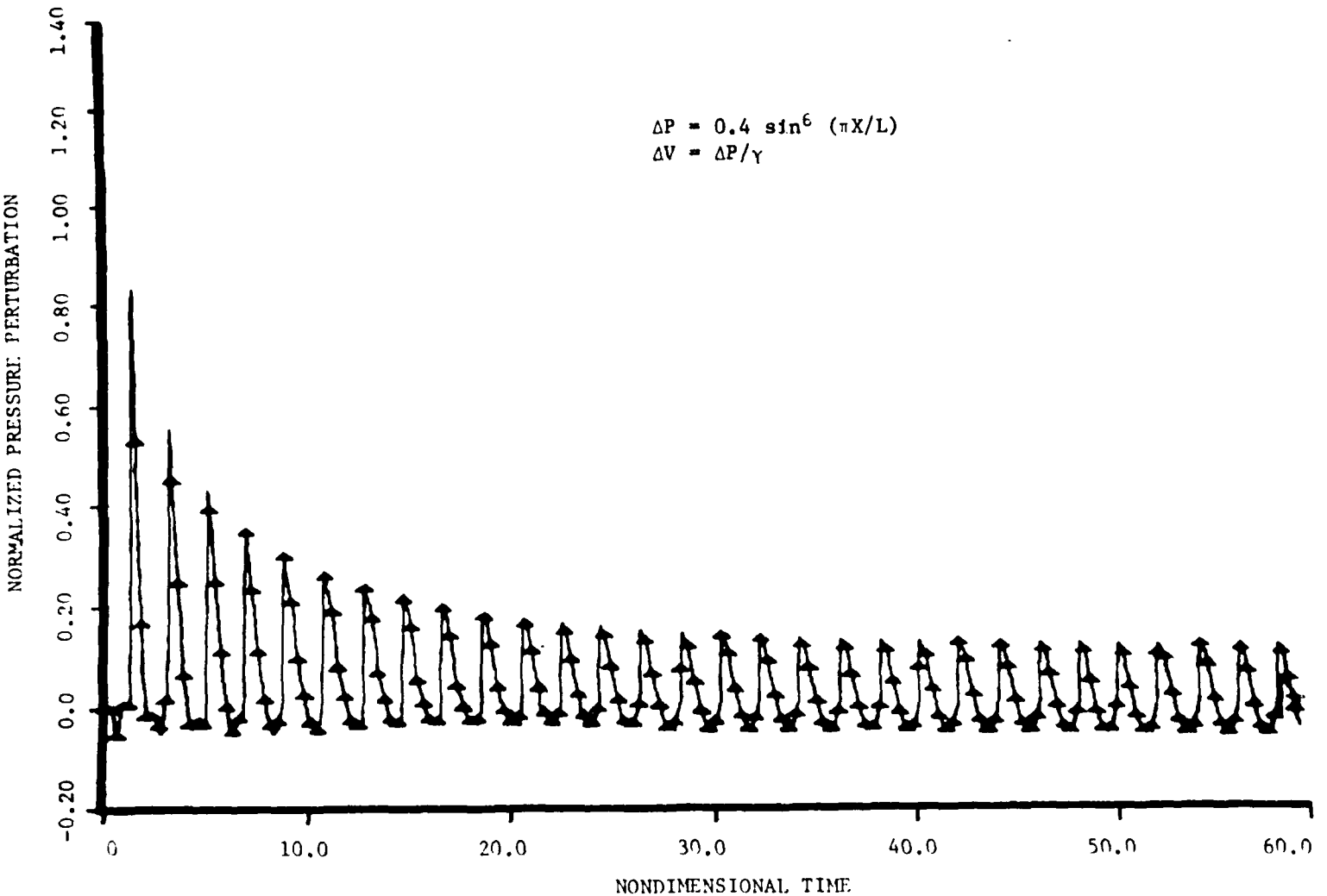

Figure 18. Time Evolution of the Normalized Oscillatory Pressure Amplitude at the Head End of the Motor for a Traveling Pulse (LW+IF+ACM).

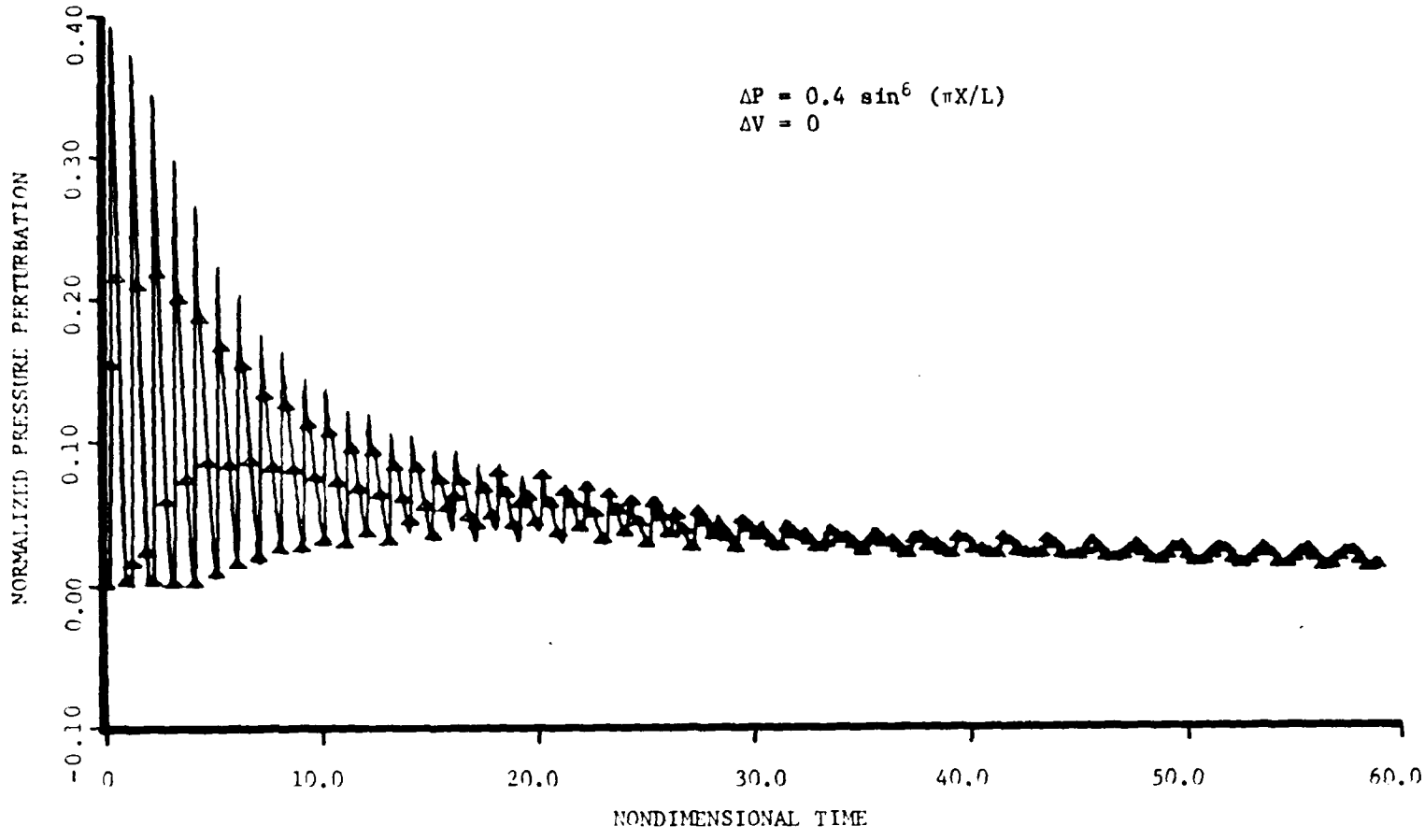

Figure 19. Time Evolution of the Normalized Oscillatory Pressure Amplitude at the Head End of the Motor for a Traveling Pulse (LW+H+ACM).

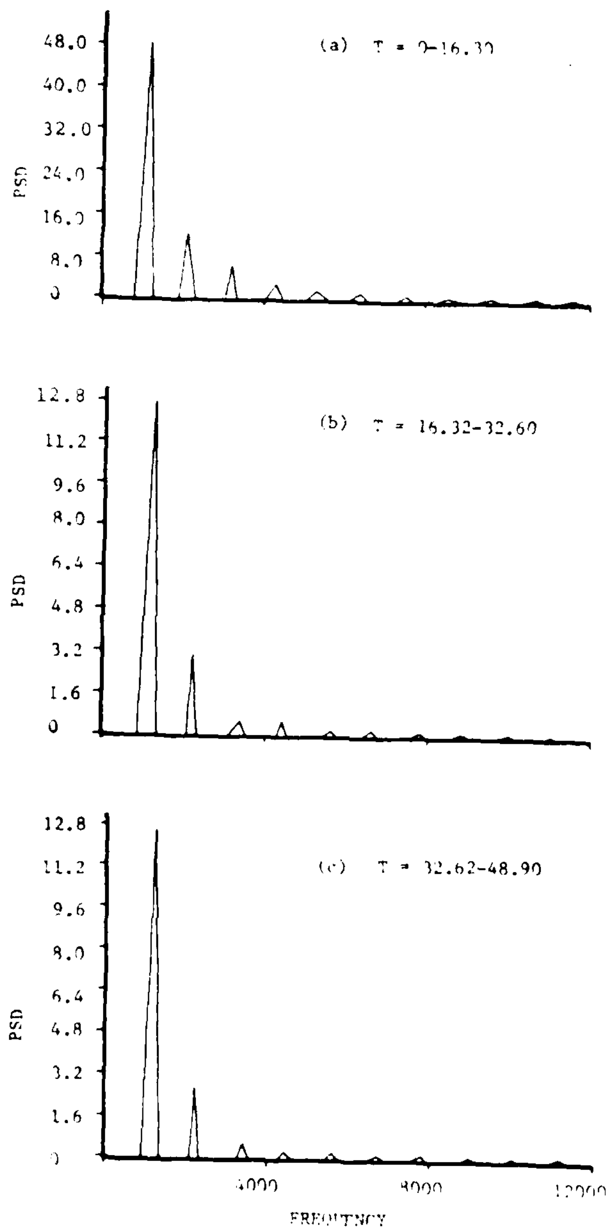

Figure 20(a) through (c). Time Evolution of Power Spectral Density as a Function of Frequency for a Traveling Pulse, P = 0.4 $\sin^6$ (X/L), [illegible] (AV+H+ACM).

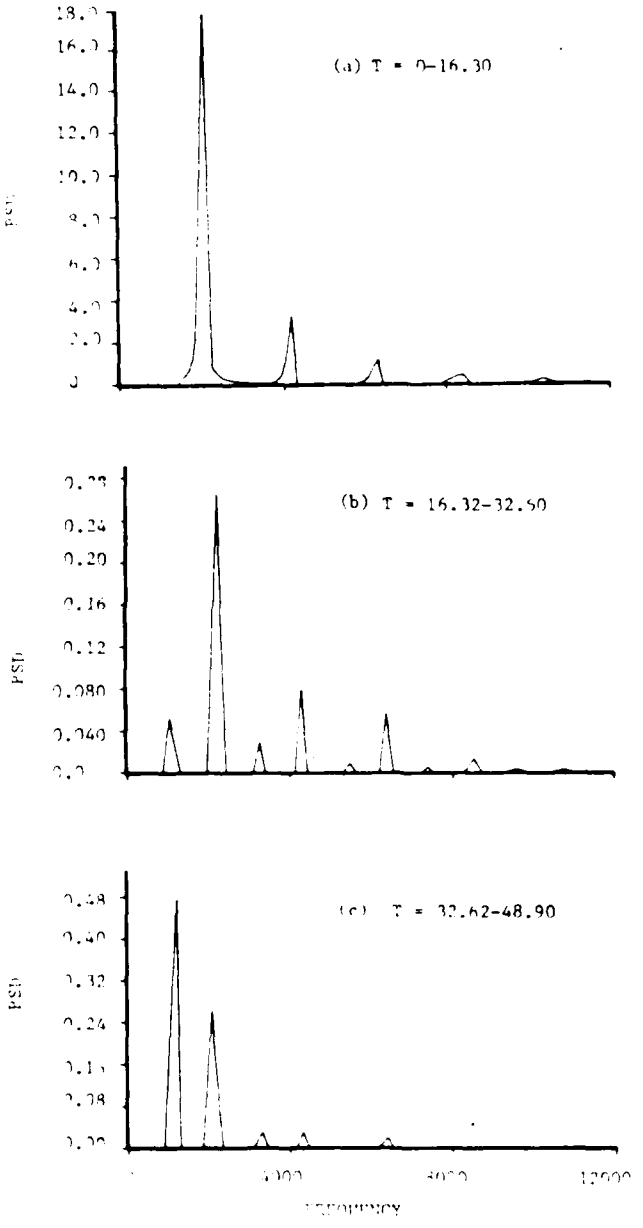

Figure 21 (a) through (c). Time Evolution of Power Spectral Density as a Function of Frequency, for a Standing Pulse, $\Delta P = 0.4\ \sin^6(\quad X)$, $V = 0$ (GAMM + XM).

SECTION 4

CONCLUSIONS

The original objective, to develop a method capable of solving steep-fronted, nonlinear instability problems in smokeless tactical rocket motors, has been accomplished.

All numerical methods introduce errors, and the numerical method and the physical problem to be solved need to be matched. For the present problem, a method based on the combination of the Lax-Wendroff, Hybrid, and Artificial Compression schemes was found to be superior to the other schemes tested. It has been shown that this scheme is capable of resolving a shock as a sharp discontinuity without generating artificial pre- or post-shock oscillations. The method does not rely on the use of an artificial viscosity and is capable of preserving the high-frequency content of the waveforms. This combination technique can also treat the reflection of shocks from boundaries and has small diffusive and dispersive errors even after many wave cycles.

The ability to analyze spectrally the computed results was added to the nonlinear instability program. This capability simplifies the interpretation of complex waveforms and will facilitate comparisons with motor data and with the results of approximate nonlinear methods.

In addition to the amplitude, waveform, and location of the pressure pulse, the details of the associated velocity disturbance are also very important in determining motor response, even when velocity coupling is not considered.

The solution of the instability problem without particles reached a limiting amplitude seemingly independent of the initial disturbance amplitude and waveform. Earlier calculations with particles, however, showed limiting amplitude to be a strong function of the initial disturbance. Thus, it appears that nonlinear particle damping effects play a significant role in determining the limiting amplitude of an instability.

The use of artificial viscosity results in the nonphysical attenuation of the high harmonics. Thus, the use of a numerical method which relies on an artificial viscosity to damp post-shock oscillations is not recommended for problems that require the solution to extend over many wave cycles.

TABLE OF SYMBOLS

A	cross section area
a	gas only, sound speed
c_p	specific heat of gas at constant pressure
c_s	specific heat of solid propellant
F_{p_i}	particle-gas interaction force per unit volume, for the i^{th} particle group
m	mass flux from burning saface
N	number of particle groups
P	pressure
Q_{p_i}	particle gas heat transfer rate per unit volume, for the i^{th} particle group
T	temperature
T_f	flame temperature of the propellant
T_s	temperature at the propellant surface
T_∞	backwall temperature of the propellant
t	time
u	velocity
u_s	velocity of the combustion products as they enter the main flow
$u_{s_{11}}$	axial component of u_s
x	axial distance
Σ	total particle to gas weight flow ratio, $\sum_i$
β_i	particle to gas weight flow ratio of the i^{th} particle group
γ	gas only isentropic exponent
ρ	density
$\dot{r}$	mass burning rate, per unit length, per unit cross sectional area

TABLE OF SYMBOLS (Continued)

Subscripts

f	flame
g	gas
p_i	i^{th} particle group
s	at the burning surface
t	at the nozzle throat

END

DATE
FILMED

7-81

DTIC